Heliyon 10 (2024) e36579

Contents lists available at ScienceDirect

Heliyon

journal homepage: www.cell.com/heliyon

Research article

Mechanisms of Yiai Fuzheng formula in the treatment of triple-negative breast cancer based on UPLC-Q-Orbitrap-HRMS, network pharmacology, and experimental validation

Ruijie Li [a,b,1], Haoliang Ke [a,1], Pan Liu [c], Qian Yang [c], Yuxin Li [c], Longzhu Ke [a,b], Xiuping Wang [a], Chaoyan Wu [a,*], Yingwen Zhang [a,b,**]

[a] Department of Integrated Chinese and Western Medicine, Zhongnan Hospital of Wuhan University, Wuhan University, Wuhan, 430071, China
[b] College of Traditional Chinese Medicine, Hubei University of Chinese Medicine, Wuhan, 430065, China
[c] Department of Radiation and Medical Oncology, Zhongnan Hospital of Wuhan University, Wuhan University, Wuhan, 430071, China

ARTICLE INFO

Keywords:
Yiai Fuzheng formula
Triple-negative breast cancer
Network pharmacology
PI3K/Akt/ mTOR pathway
Epithelial-mesenchymal transition

ABSTRACT

Ethnopharmacological relevance: Yiai Fuzheng formula (YAFZF), as a Traditional Chinese Medicine (TCM) prescription, has been used widely at Zhongnan Hospital of Wuhan University for its therapeutic effects and high safety on triple-negative breast cancer (TNBC).

Objective: In this study, we employed ultra-high-performance liquid chromatography-quadrupole/orbitrap high-resolution mass spectrometry (UPLC-Q-Orbitrap-HRMS), network pharmacology, and experimental validation to elucidate the underlying action mechanism of YAFZF in the treatment of TNBC.

Methods: The key active ingredients in YAFZF were analyzed using UPLC-Q-Orbitrap-HRMS, and then the potential components, target genes and signalling pathways of YAFZF were predicted using the network pharmacological method. We then used molecular docking to visualize the combination characteristics between major active components and macromolecules in the crucial pathway. *In vitro* experiments were conducted to investigate the inhibitory effects of YAFZF treatment on the cell viability, invasion, and migration of 4T1 and MDA-MB-231 cells. The xenograft TNBC models were constructed using female Balb/c mice, and their body weights, tumour volumes, and weights were monitored during YAFZF treatment. Quantitative real-time PCR (qRT-PCR), Hematoxylin-eosin (HE), immunohistochemistry (IHC) staining, Western blot (WB), and terminal deoxynucleotidyl transferase (TdT)-dUTP nick-end labeling (TUNEL) staining were used for further experimental validation.

Results: Based on UPLC-Q-Orbitrap-HRMS and network pharmacology analysis, 6 major bioactive components and 153 intersecting genes were obtained for YAFZF against TNBC. Functional enrichment analysis identified that the phosphatidylinositol 3-kinase (PI3K)-protein kinase B (Akt) signalling pathway might be the mechanism of action of YAFZF in the treatment of TNBC. Molecular docking results suggested that the main active compounds in YAFZF had strong binding energies with the proteins in the PI3K/Akt pathway. *In vitro* experiments showed that YAFZF inhibited the cell viability, invasion, and migration abilities of TNBC cells. Animal

* Corresponding author.
** Corresponding author. Department of Integrated Chinese and Western Medicine, Zhongnan Hospital of Wuhan University, Wuhan University, Wuhan, 430071, China.
E-mail addresses: grace98765@163.com (C. Wu), hhao3838@sina.com (Y. Zhang).
[1] The authors contributed equally to this work.

https://doi.org/10.1016/j.heliyon.2024.e36579
Received 21 June 2024; Received in revised form 17 August 2024; Accepted 19 August 2024
Available online 20 August 2024

experiments confirmed that YAFZF treatment suppressed tumour cell proliferation and increased apoptotic cells. PCR, HE, WB, and IHC results indicated that YAFZF could suppress xenograft tumour metastases by inhibiting the PI3K/AKT/mTOR pathway regulating the epithelial-mesenchymal transition (EMT) process.

Conclusion: YAFZF therapy showed its potential for reducing proliferation, invasion, and migration abilities, increasing apoptosis of TNBC cells. Furthermore, YAFZF treated TNBC by inhibiting xenograft tumour distant metastases via the regulation of EMT by the PI3K/Akt/mTOR pathway, suggesting that it may be useful as an adjuvant treatment.

Abbreviations

AGE	advanced glycation end products
AKT	protein kinase B
AOD	average optical density
AR	androgen receptor
BC	breast cancer
BP	biological process
CASP3	caspase-3
CC	cellular component
CCND1	cyclin D1
DAB	diaminobenzidine
DL	drug-likeness
EGFR	epidermal growth factor receptor
EMT	epithelial-mesenchymal transition
ER	estrogen receptor
ERBB2	receptor tyrosine-protein kinase erbB-2
ESR1	Estrogen receptor 1
FoxO	Forkhead box O
HE	Hematoxylin-eosin
HER	Human epidermal growth factor receptor
HIF1	Hypoxia-inducible factor 1
HnRNPA2	heterogeneous ribonuclear protein A2/B1
HRAS	HRas proto-oncogene GTPase
HSP90AA1	Heat shock protein HSP 90-alpha
IHC	Immunohistochemistry
IL6	interleukin-6
JUN	Jun proto-oncogene
KEGG	Kyoto Encyclopedia of Genes and Genomes
KYP	Kaiyu powder
LC/MS	liquid mass chromatography-mass spectrometry
MAPK	mitogen-activated protein kinases
MF	molecular function
MW	molecular weight
OB	oral bioavailability
OMIM	Online Mendelian Inheritance in Man
PI3K	Phosphatidylinositol 3-kinase
PIK3CA	Phosphatidylinositol 4,5-bisphosphate 3-kinase catalytic subunit alpha isoform
PIP2	Phosphatidylinositol (4,5)-bisphosphate
PIP3	Phosphatidylinositol (3,4,5)-trisphosphate
PMSF	phenylmethanesulfonyl fluoride
PPI	protein-protein interaction
PR	progesterone receptor
qRT-PCR	quantitative real-time PCR
SIRT1	Sirtuin 1
SRC	proto-oncogene tyrosine-protein kinase Src
STAT3	signal transducer and activator of transcription 3
TCM	traditional Chinese medicine
TCMSP	traditional Chinese medicine systems pharmacology
TdT	terminal deoxynucleotidyl transferase
TFs	transcription factors
TNBC	triple-negative breast cancer
TNF	tumor necrosis factor
TP53	tumor protein p53
TTD	Therapeutic Target Database
TUNEL	terminal deoxynucleotidyl transferase dUTP nick-end labeling
UPLC-Q-Orbitrap-HRMS	ultra-high-performance liquid chromatography–quadrupole/orbitrap high–resolution mass spectrometry
VEGFA	vascular endothelial growth factor A
WB	Western blot
YAFZF	Yiai fuzheng formula

1. Introduction

Triple-negative breast cancer (TNBC) is a rare and aggressive breast cancer (BC) that lacks estrogen receptors (ER), progesterone receptors (PR), and human epidermal growth factor receptors (HER) 2. This type of cancer accounts for 15–20 % of all BC cases and is more aggressive and invasive, with an earlier onset and a poor prognosis [1]. Unlike other BC subtypes, TNBC is more likely to recur and metastasize, more easily occurring in distant sites, such as the lung, liver, and brain [2,3]. Due to limited clinical treatment options and a lack of targeted therapies, TNBC patients have a low survival rate [4]. Therefore, the active search for effective treatments for TNBC is vital.

Traditional Chinese medicine (TCM) is an effective complementary therapy for cancer because it promotes body energy, regulates metabolic pathways, and inhibits tumour cell proliferation [5]. It is recorded in the book "The Secret of the Cave" that Kaiyu powder (KYP) can effectively prevent and treat mammary gland hyperplasia and BC [6]. Yiai Fuzheng formula (YAFZF), which supplemented KYP with some meridian tropism, anti-cancer agents associated with mammary glands, was developed to optimize the treatment efficacy for TNBC. The whole YAFZF consists of 16 herbs: *Astragalus membranaceus* (Fisch.) *Bunge.* (Huang Qi), *Poria cocos* (Schw.) *Wolf fruit* (Fu Ling), *Lycopodium japonicum* Thunb. (Shen Jin Cao), *Luffa cylindrica* (L.) M. Roem. (Si Gua Luo), *Laminaria japonica* (Kun Bu), *Fritillaria thunbergii* Miq. (Zhe Bei Mu), *Rohdea chinensis* (Baker) N. Tanaka (Kai Kou Jian), *Sparganium stoloniferum* (Graebn.) Buch.-Ham. ex Juz. (San Leng), *Curcuma phaeocaulis* Valeton (E Zhu), *Whitmania pigra* Whitman (Shui Zhi), *Curcuma longa* L. (Yu Jin), *Prunella vulgaris* L. (Xia Ku Cao), *Oldenlandia diffusa* (Willd.) Roxb. (Bai Hua She She Cao), *Taraxacum officinale* (L.) Weber ex F.H.Wigg. (Pu Gong Ying), *Gleditsia sinensis* Lam. (Zao Jiao Ci), *Sargentodoxa cuneata* (Oliv.) Rehder & E.H.Wilson (Hong Teng). Among these herbs, *Astragalus membranaceus* (Fisch.) *Bunge.* has been used to treat multiple diseases by protecting against oxidative stress, inflammation, apoptosis, and fibrosis. Its anti-cancer properties are attributed to the activation of the immune system, inhibiting invasion, and preventing cancer cells from metastasizing [7]. *Rohdea chinensis* (Baker) N. Tanaka is described as a cancer-treating herb in the Chinese Materia Medica Dictionary. The agent inhibits cell cycle and migration and induces apoptosis as part of its anti-cancer activity [8]. *Sparganium stoloniferum* (Graebn.) Buch.-Ham. Ex Juz. and *Curcuma phaeocaulis* Valeton have been proven to be more effective when used in combination with TCM history on tumours, thrombotic conditions, estrogen symptoms, and pain [9]. *Sargentodoxa cuneata* (Oliv.) Rehder & E.H.Wilson has long been used for treating inflammation, rheumatism, and appendicitis, and its extract might make tumour treatments more effective and less toxic [10]. A combination of YAFZF and other treatments has shown significant effects in clinical trials for treating TNBC patients. A previous study found that Chinese herbs contained in YAFZF inhibit cancer cell proliferation and induce caspase-3(CASP3)-mediated apoptosis in metastasis BC cells [11]. YAFZF appears to be a promising treatment option for TNBC, but its mechanism of action needs to be further elucidated.

From a comprehensive, holistic, and predictive perspective, network pharmacology reveals that multiple targets, networks, and disease modules drive disease [12]. A large number of experimental data indicate that TCM network pharmacology could explain the deep mechanism as to why diseases and syndromes arise and develop, thus exploring the combination law and traditional efficacy mechanism of TCM formula, which may lead to more accurate TCM therapeutic interventions [13–15].

The main active ingredients of YAFZF were determined using ultra-high-performance liquid chromatography-quadrupole/orbitrap high-resolution mass spectrometry (UPLC-Q-Orbitrap-HRMS). Following that, we used TCM network pharmacological techniques and molecular docking to predict and visualize potential target genes and signalling pathways that might be involved in the action of YAFZF on TNBC. The *in vitro* and *in vivo* experiments confirmed the therapeutic effects and mechanisms of YAFZF against TNBC,

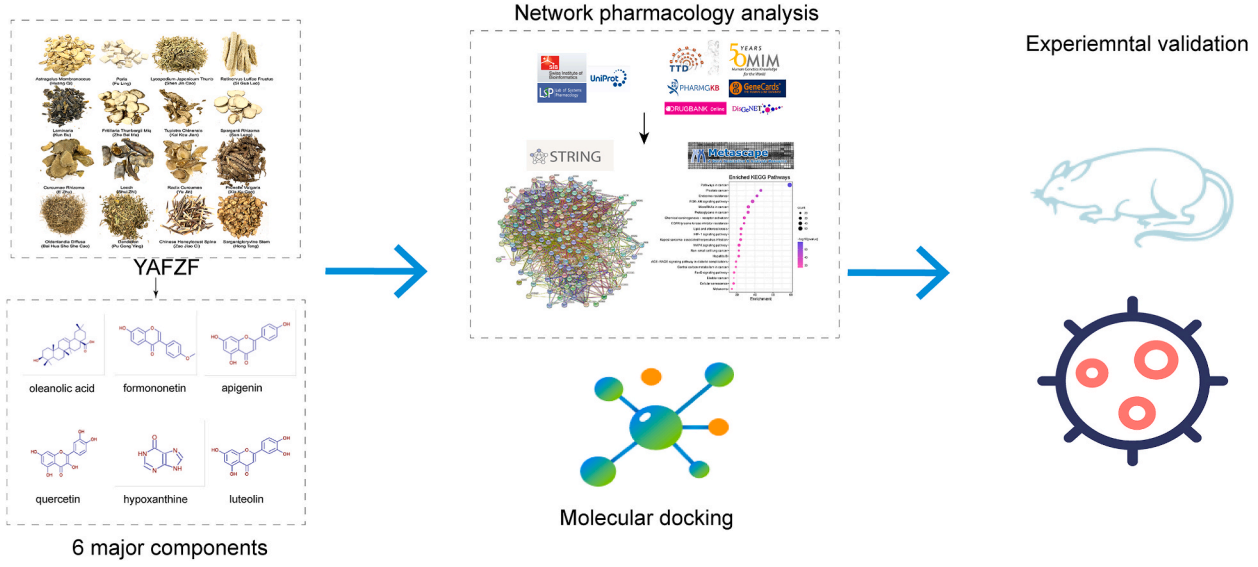

Fig. 1. Flowchart of the study.

demonstrating its clinical utility (Fig. 1).

2. Materials and methods

2.1. Herbal sample preparation and administration

Obtaining the herbs from Hubei Chenmei Chinese Traditional Medicine Co., Ltd. (Huanggang, China), we soaked all of these herbs (Table 1) proportionally in ultrapure water for 60 min and brought the combination to boil at 40–90 °C in an imported vacuum environment (Jingxi, South Korea). The mixture was decocted for 1 h, concentrated, and extracted for 200 μL of supernatant using a vacuum system. The supernatant was mixed with 1000 μL of 80 % methanol (Thermo Fisher Scientific, China), eddied, and centrifuged for 10 min at 4 °C. The supernatant was filtered to remove residue and stored at −80°Cuntil UPLC-Q-Orbitrap HRMS analysis. Moreover, the original herbs of YAFZF were soaked proportionally in 2500 mL of ultrapure water for 60 min. Then, the mixture was heated and concentrated to produce 49 mL of herbal solution in a vacuum system. The final concentration of herbal medicine solution was 4.4 g/ml and stored at 4 °C.

2.2. Quantitative analysis of major components of YAFZF based on UPLC-Q-Orbitrap-HRMS

In the liquid chromatography-mass spectrometry (LC/MS) detection of Chinese medicinal solution, an UltiMate 3000 RS Chromatography system (Thermo Fisher Scientific, China) was utilized in conjunction with Q Exactive Orbitrap High-Resolution Mass Spectrometer (Thermo Fisher Scientific, China). The AQ-C18 column (150 × 2.1 mm, 1.8 μm) (Shanghai Welch, China) was used for chromatographic separation with a flow rate of 0.30 mL/min at 35 °C. To finish chromatographic gradient elution, 0.1 % formic acid (A) (Shanghai Aladdin Biochemical Technology Co., Ltd., China) and methanol (B) were added to the mobile phase (Table 2). For MS analysis and identification, we used a full scope of (100.0 ~ 1500.0 *m/z*) and a resolution of 70000/17500 of full mass/dd-MS2 scan with positive and negative ion switching patterns. The specific parameters include a source of ions, an electrospray ionization source, spay voltage of 3.2 KV (positive), capillary temperature of 300 °C, collision gas of high purity argon, sheath gas (N2) flow rate of 40 Arb, and auxiliary gas (N2) flow rate of 15 Arb at 350 °C. The data was collected in 30 min and organized using CD2.1 (Thermo Fisher Scientific, China), then searched and compared in the mzCloud database.

2.3. Network pharmacological research

2.3.1. Screening of active components of YAFZF and related targets

Using the herbal names of YAFZF as keywords, we found the active components in TCMSP (https://tcmspw.com/tcmsp.php) [16]. In addition to *Luffa cylindrica* (L.) M. Roem., *Rohdea chinensis* (Baker) N. Tanaka, *Whitmania pigra* Whitman, and *Taraxacum officinale* (L.) Weber ex F.H.Wigg., whose active ingredients could not be obtained from TCMSP. The chemical structures of these herbs were identified through a literature search, and the final effective active components were confirmed by SwissADME (http://www.swissadme.ch) [17] and Lipinski Rules: lipophilic index (Log*P*≤5); molecular weight (MW) ≤500; number of OH + NH bonds≤5; number of Ns and Os ≤ 10. To obtain similar targets, SwissTargetPrediction (http://www.swisstargetprediction.ch) [18] was utilized to predict all active components. Predicted target genes were standardized based on the UniProt database (http://www.uniprot.org/) [19]. The "herb-component-target" network was visualized, analyzed, and constructed using Cytoscape 3.7.2 software (UC, Gladstone Institute, University of Toronto, etc., CA, USA).

Table 1
Herbs in YAFZF.

Chinese name	Scientific name	Dosage(g)	Origin (China)
Huang Qi	*Astragalus membranaceus* (Fisch.) *Bunge.*	15	Shanxi
Fu Ling	*Poria cocos* (Schw.) *Wolf fruit*	15	Yunnan
Shen Jin Cao	*Lycopodium Japonicum* Thunb.	12	Hubei
Si Gua Luo	*Luffa cylindrica* (L.) M.Roem.	15	Zhejiang
Kun Bu	*Laminaria japonica*	12	Zhejiang
Zhe Bei Mu	*Fritillaria Thunbergii* Miq.	15	Zhejiang
Kai Kou Jian	*Rohdea chinensis* (Baker) N.Tanaka	9	Hubei
San Leng	*Sparganium stoloniferum* (Graebn.) Buch.-Ham. ex Juz.	15	Jiangsu
E Zhu	*Curcuma phaeocaulis* Valeton	15	Sichuan
Shui Zhi	*Whitmania pigra* Whitman	6	Shandong
Yu Jin	*Curcuma longa* L.	15	Zhejiang
Xia Ku Cao	*Prunella vulgaris* L.	15	Henan
Bai Hua She She Cao	*Oldenlandia diffusa* (Willd.) Roxb.	15	Jiangxi
Pu Gong Ying	*Taraxacum officinale* (L.) Weber ex F.H.Wigg.	15	Zhejiang
Zao Jiao Ci	*Gleditsia sinensis* Lam.	15	Henan
Hong Teng	*Sargentodoxa cuneata* (Oliv.) Rehder & E.H.Wilson	12	Jiangxi

Table 2
Chromatography gradient.

Time(min)	A (%)	B(%)
1	98	2
5	80	20
10	50	50
15	20	80
20	5	95
27	5	95
28	98	2
30	98	2

2.3.2. Screening of related targets for TNBC

To gather related target data, we searched GeneCards (http://www.genecards.org/) [20], PharmGKB (http://www.pharmgkb.org/) [21], Online Mendelian Inheritance in Man (OMIM) (http://www.omim.org/) [22], Therapeutic Target Database (TTD, http://db.idrblab.net/ttd/) [15,23], DisGeNET (https://www.disgenet.org/) [24] and DrugBank (http://go.drugbank.com/) 6 online databases. Duplicate targets were eliminated to obtain TNBC-related targets.

2.3.3. Protein-protein interaction (PPI) network establishment

All predicted targets of YAFZF were intersected with related targets of TNBC, and the intersecting target genes were subsequently imported into the STRING database (https://string-db.org/) [25]. The parameters involved in STRING database analysis are as follows: (1) Full STRING network as the network type; (2) Evidence as the meaning of network edges; (3) Medium confidence (0.400) as the minimum required interaction score; (4) Network display options: hide disconnected nodes in the network. A PPI network diagram was built after free targets were eliminated and the targets were restricted to "human species". The key targets were identified by analyzing the PPI network file using the Network Analyzer function of the Cytoscape 3.7.2 software.

2.3.4. Kyoto encyclopedia of genes and genomes (KEGG) and GO enrichment analyses

Subsequently, the PPI network targets were uploaded onto the Metascape website(https://metascape.org/) [26] for analysis of GO function enrichment and KEGG pathway enrichment. Enrichment results were filtered by $P < 0.05$ and then sorted based on count values. Bioinformatics (http://www.bioinformatics.com.cn/) [27], showed the top 20 GO entries for BP, CC, and MF, and the top 20 KEGG entries.

2.4. Molecular docking analysis

Through LC/MS analysis, mzCloud database best match ranking, and literature search, we identified YAFZF's key active components. Small molecule SDF structures were obtained from PubChem (https://pubchem.ncbi.nlm.nih.gov) [28] and converted to PDB format files using Open Babel (http://openbabel.org). The RCSB Protein Data Bank provided protein PDB structures (PIK3CA:7JIU; AKT1:1UNQ) (http://www.rcsb.org/pdb/) [29]. With AutoDock Tools 1.5.7 software, target proteins and small molecules were docked and determined binding ability. The docking results were visualized using PyMOL 2.5.0 software and bioinformatics (http://www.bioinformatics.com.cn/).

2.5. Cell culture

Mouse fibroblast NIH/3T3, normal liver cell NCTC 1469, TNBC cell line 4T1 and MDA-MB-231 were purchased from Procell Life Science&Technology Co., Ltd. (CL-0007, CL-0150; Wuhan, China). The cells were cultivated in RPMI-1640 medium (HyClone, Logan, Utah, USA) with 10 % fetal bovine serum (FBS) (Invitrogen, USA) and 1 % penicillin/streptomycin (Biosharp, China) in 5 % CO_2 at 37 °C. The YAFZF employed in the *in vitro* experiment was diluted with PBS (HyClone, Logan, Utah, USA) to the corresponding concentration to stimulate cells for 24 h.

2.6. Reagents and antibodies

The following reagents were used: phosphatidylinositol 3-kinase (PI3K) agonist 740 Y-P (HY-P0175, MedChemExpress, NJ, USA); Primers (Beijing Tsingke Biotech Co., Ltd. Beijing, China); Phenylmethanesulfonyl fluoride (PMSF) (BL507A, Biosharp Biotechnology, Hefei, China); Buffer for RIPA lysis (P0013B), Assay kit for BCA protein analysis (P0012) (Beyotime Biotechnology, Shanghai, China); phosphorylase inhibitor, hematoxylin and eosin (Servicebio Technology Co., Ltd. Wuhan, China). Primary antibodies used in the work including:β-actin(66009-1-lg), PI3K(20584-1-AP),AKT(10176-2-AP),p-AKT(80455-1-RR), Vimentin (10366-1-AP), E-cadherin (20874-1-AP),mTOR(66888-1-lg),p-mTOR(67778-1-lg) (Proteintech, Wuhan, China); p-PI3K (#4228) and SNAIL (#3879) (Cell Signalling Technology, MA, USA); TWIST (RT1635) (Huaan Biotechnology Co., Ltd. Hangzhou, China).

2.7. Cell viability assay

The 4×10^3 cells were seeded in a 96-well plate and exposed to varying doses of YAFZF for 24 h and 48 h, respectively. Following that, 10 μL of the cell counting kit-8 (CCK-8) (MeilunBio, China) was added to each well before incubation for 0.5–4 h. To detect the absorbance at 450 nm, a microplate reader (SpectraMax M2, Molecular Devices, China) was utilized. Based on the half maximal inhibitory concentration (IC50) values of YAFZF, the cell experiment was divided into six groups: control group, 740 Y-P group (25 μg/ml), YAFZF low-dose group (15 mg/ml), YAFZF medium-dose group (30 mg/ml), YAFZF high-dose group (60 mg/ml), and YAFZF medium-dose plus 740 Y-P group (25 μg/ml).

2.8. Transwell invasion and migration assay

The cells were incubated in a 6-well plate with an inoculation density of 1.2×10^5 cells/well and stimulated with PI3K agonist 740Y-P for 24 h. These cells were replated in a 24-well plate with 8 μm size transwell system after being exposed to a 24-h treatment of YAFZF. For the invasion assay, a 20 % FBS medium was put into the lower compartment, and a density of 1×10^5 cells with FBS-free medium were seeded into the upper chamber following coating with Matrix-Gel (C0372, Beyotime Biotechnology, Shanghai, China). For migration assay, these treated cells were planted with serum-free medium (5×10^4 cells) in the upper chamber and the following procedures were similar to the invasion assay. After incubation for 48 h, the cells on the underside were fixed with 4 % paraformaldehyde and then stained with 0.1 % crystal violet for 20 min, respectively. The stained cells were photographed and counted under a light microscope (Olympus, Tokyo, Japan; magnification: 100×). The number of invaded or migrated cells was quantified by using Image J software to count the number of cells from 15 random fields.

2.9. Animal, xenograft model establishment and drug administration

Upon approval of Wuhan University's Zhongnan Hospital Experimental Animal Welfare Ethics Committee, all animal experiments were conducted (Approval No. ZN2022059). This study used six-week-old female Balb/c mice obtained from SiPeiFu (Beijing) Biotechnology Co., Ltd., and housed in a setting with a stable temperature (22–25 °C), humidity (50 %), and 12-h light/dark cycle. The TNBC xenograft model was developed by injecting 2×10^5 4T1 cells suspended in an FBS-free medium into the left fourth mammary pad of each mouse. When tumour volume reached 50 mm^3(volume = length × $width^2$ × 0.52), mice were randomly divided into four groups to determine YAFZF's therapeutic effects. According to the equivalent dose ratio of body surface area, we determined the animal dosage (g/kg) on the basis of human dosage multiplying the conversion factor (12.3). For the treatment groups, 11.07 g/kg, 22.14 g/kg, and 44.28 g/kg of 200 μL YAFZF herbal solutions were administered intragastrically. Meanwhile, a 0.9 % sterile saline solution was gavaged once a day for 14 days to the mice in the model group. During treatment, all mice were weighed and measured every two days. On day 23, the whole lung, liver, and tumour of each mouse were collected, and their tumours were weighed simultaneously after sacrifice.

2.10. Quantitative real-time PCR (qRT-PCR)

The Trizol reagent (Vazyme, Nanjing, China) was utilized to extract total RNA from tumour tissues, and Synthesis Supermix (Yeasen Biotechnology Co., Ltd., Shanghai, China) was used to synthesize cDNA. For further amplification and detection, we mixed SYBR Green I, cDNA, and gene-specific primers with the FastSYBR Mixture PCR Kit (CWBIO, China) instructions and put them into Fluorescent Quantitative CFX96 Real-Time PCR System (Bio-Rad Laboratories, CA, USA). Taking β-actin as the control gene, miRNA expressions of target genes were measured based on the $2^{-\Delta\Delta CT}$ method. Table 3 shows the primers used for the target genes.

2.11. Hematoxylin-eosin (HE) analysis

The lung and liver tissues of mice were fixed in 4 % paraformaldehyde for 48 h. The tissues were embedded in paraffin and then sectioned at a thickness of 5 μm. After deparaffinizing, these slices were washed with water. Hematoxylin and eosin dye liquor were applied to lung and liver sections for 5 min, followed by dehydration and sealing. Observations and acquisitions of lung and liver images were conducted using a microscope (Olympus, Tokyo, Japan) and OLYMPUS cellSens Entry 3.1 software. The metastasis ratios

Table 3
The primer sequences of target genes.

Gene	Sequences (5′-3′)
Vimentin	Forward: GACCTCTACGAGGAGGAGAT
	Reverse: TTGTCAACATCCTGTCTGAA
SNAIL	Forward: CACACGCTGCCTTGTGTCT
	Reverse: GGTCAGCAAAAGCACGGTT
TWIST	Forward: CAGCTACGCCTTCTCGGTCT
	Reverse: CTGTCCATTTTCTCCTTCTCTG
β-actin	Forward:GCCACCCAGAAGACTGTGGAT
	Reverse: TGGTCCAGGGTTTCTTACTCC

in histological sections were calculated using Image J software (National Institutes of Health, MD, USA).

2.12. Western blot (WB)

Using RIPA, PMSF, and phosphorylase inhibitors at a ratio of 100:1:1, tumour tissues were lysed, and their concentrations were measured and then boiled with a loading buffer for 10 min. Afterward, these samples were concentrated, separated, shifted to PVDF membranes (Millipore, USA), and blocked for 60 min with 5 % Albumin Bovine (4240GR100, Biofroxx, Germany). Afterward, primary antibodies were incubated at 4°C overnight. On the second day, TBST buffer was used to wash the membranes thrice at 10-min intervals. The membranes were incubated with secondary antibodies for 60 min at room temperature. Immune bands were observed using an enhanced chemiluminescent detection kit (Bio-Rad Laboratories, CA, USA).

2.13. Immunohistochemistry (IHC) staining

Paraformaldehyde-fixed tissues were deparaffinized in xylene and washed with distilled water. Following antigen retrieval and blocking, tumour sections were incubated with primary antibodies against Ki67 (1:500), Vimentin (1:500), E-cadherin (1:400), and SNAIL (1:300), and secondary antibodies conjugated to HRP at room temperature for 120 min and 60 min, respectively. After three 5-min intervals of PBST rinsing, the tumor sections were stained with hematoxylin dye liquid and diaminobenzidine (DAB) from Maxin Biotech, LTD. in Fuzhou, China. These stained images were taken using a bright field of microscope using OLYMPUS cellSens Entry 3.1 software (Olympus, Tokyo, Japan). The average optical density (AOD) values for Vimentin, E-cadherin, and SNAIL were calculated using Image J.

2.14. Terminal deoxynucleotidyl transferase (TdT)-dUTP nick-end labeling (TUNEL) assay

Deparaffinization of tissue sections was performed using xylene and absolute ethyl alcohol. After boiling in citric acid antigen repair buffer (pH 6.0), the sections were washed three times in PBS (pH 7.4). A mixture of TdT and dUTP at a 1:10 ratio was applied overnight at 4 °C according to the TUNEL staining assay kit (11684817910, Roche, Basel, Switzerland). After three PBS washes, the sections were stained for 10 min at room temperature in the dark using DAPI solution (C1002, Beyotime, Shanghai, China). The sections were sealed with Fluoromount-G (0100-01, SouthernBiotech, Birmingham, USA), and imaged with a fluorescent microscope (Nikon, Tokyo, Japan) and Pannoramic Scanner 2.1.2 software.

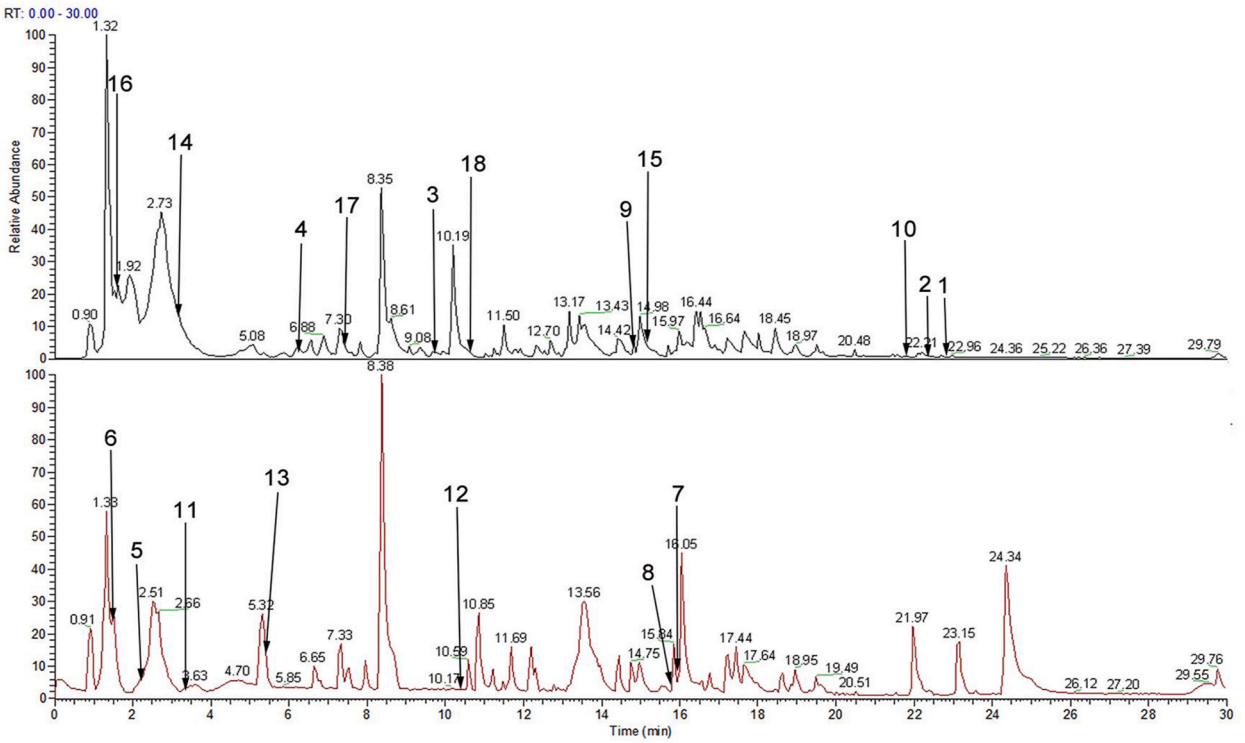

Fig. 2. Total ion chromatogram and major active components analysis of YAFZF by UPLC-Q-Orbitrap-HRMS. Black showed the total ion chromatogram of the negative mode; red showed the total ion chromatogram of the positive mode.

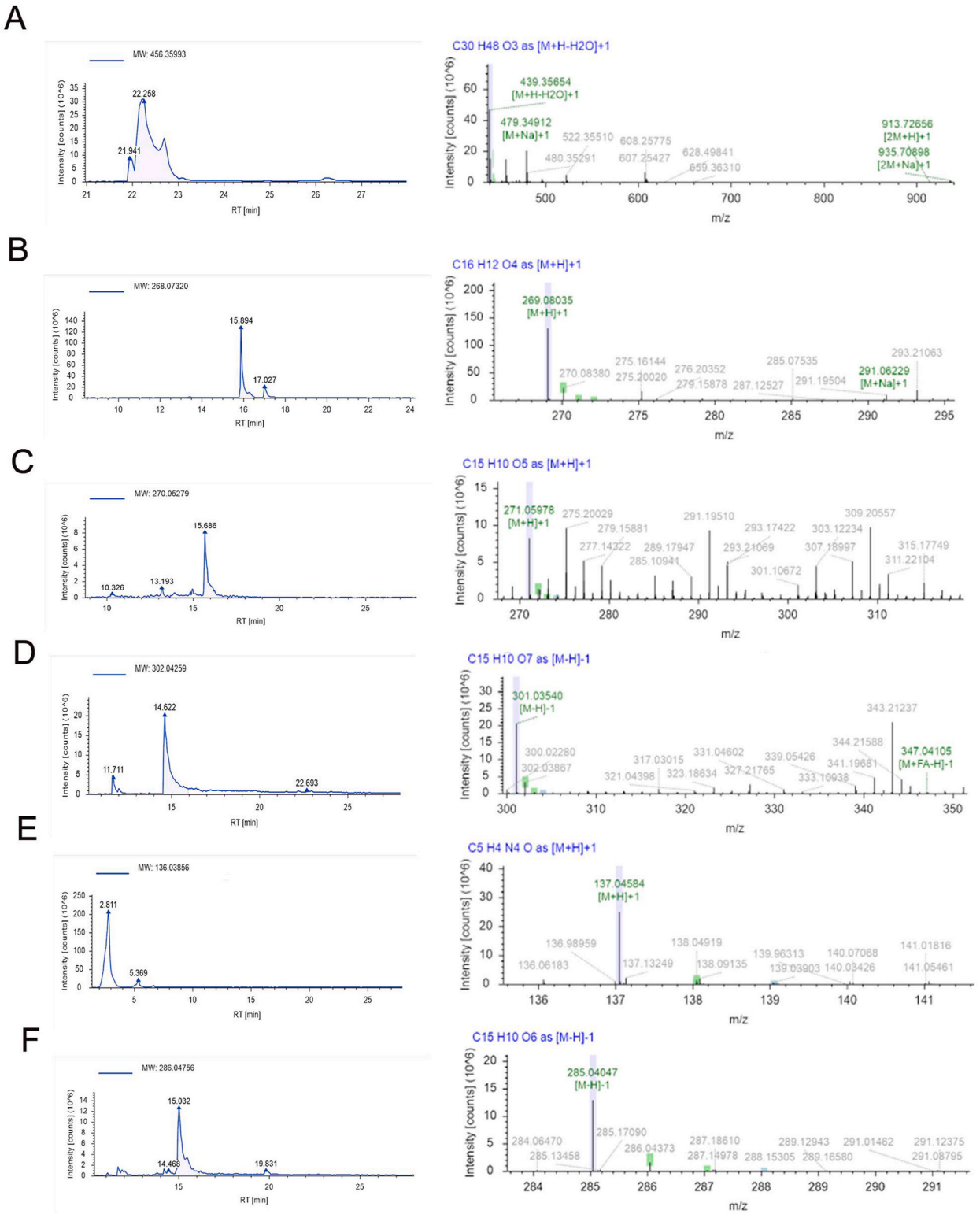

Fig. 3. The relative molecular weights and MS structural analyses of oleanolic acid (A), formononetin(B), apigenin(C), quercetin(D), hypoxanthine (E), and luteolin(F).

2.15. Statistical analysis

After three independent experiments, data are presented as a mean ± SD. Prism 8.0.2 software (GraphPad, CA, USA) was utilized for statistical analysis to compare different groups based on student's t-tests and one-way ANOVA. Statistical significance was presented by a P value < 0.05.

3. Results

3.1. UPLC-Q-Orbitrap-HRMS analysis of YAFZF

In the mzCloud database, the YAFZF sample solution matched 628 components, and the best match scores for 372 components exceeded 60. Compound structures with more than 80 mzCloud best match scores were analyzed using LC/MS [30]. It was only oleanolic acid, formononetin, apigenin, quercetin, hypoxanthine, and luteolin that ranked in the top mzCloud best match score, with high content in Chinese herbal medicine and were proven therapeutic effectiveness based on searching documents [31–35]. Therefore, the six small molecular components were crucial to the therapeutic efficacy of YAFZF (Table S1). Due to its good peak shape, 0.1 % formic acid was chosen to mix with water to analyze these small molecular components. Mobile phase and full mass/dd-MS2 scans helped collect ion peaks and improve ionization efficiency. Formononetin, apigenin, and hypoxanthine peaks were collected using positive ion mode, while the remaining three components were collected using negative ion mode. After the total 30 min running time of chromatography analysis, retention times of 18 common Chinese medicine components were shown in Fig. 2 and their mass spectrometry parameters were shown in Table S2. In terms of MS structural analysis, relative molecular weights and MS1 structures of oleanolic acid (Fig. 3A), formononetin (Fig. 3B), apigenin (Fig. 3C), quercetin (Fig. 3D), hypoxanthine (Fig. 3E), and luteolin (Fig. 3F) were analyzed separately.

3.2. Active ingredients and target-disease network construction in YAFZF

Firstly, we input every herbal name in the Traditional Chinese Medicine Systems Pharmacology (TCMSP) database and screen their main components based on OB $\geq$ 30 % and DL $\geq$ 0.18. Subsequently, we incorporated all components and deleted the duplicated parts to obtain a total of 73 ingredients and 185 targets for YAFZF. The literature search also revealed 4 active ingredients and 79 targets for *Luffa cylindrica* (L.) M. Roem.; 10 active ingredients and 610 targets for *Rohdea chinensis* (Baker) N. Tanaka; 17 active ingredients and 960 targets for *Taraxacum officinale* (L.) Weber ex F.H.Wigg.; 11 active ingredients and 253 targets for *Whitmania pigra* Whitman. In total, 109 active ingredients and 920 targets were obtained after combining and removing duplicate values for 16 herbs in YAFZF (Fig. 4A).

A total of 688 gene targets related to TNBC were identified in disease databases. A "drug-target-disease" network (Fig. 4B), consisting of 248 nodes and 1621 edges, was built using Cytoscape 3.7.2 software to clarify the therapeutic effects of YAFZF on TNBC.

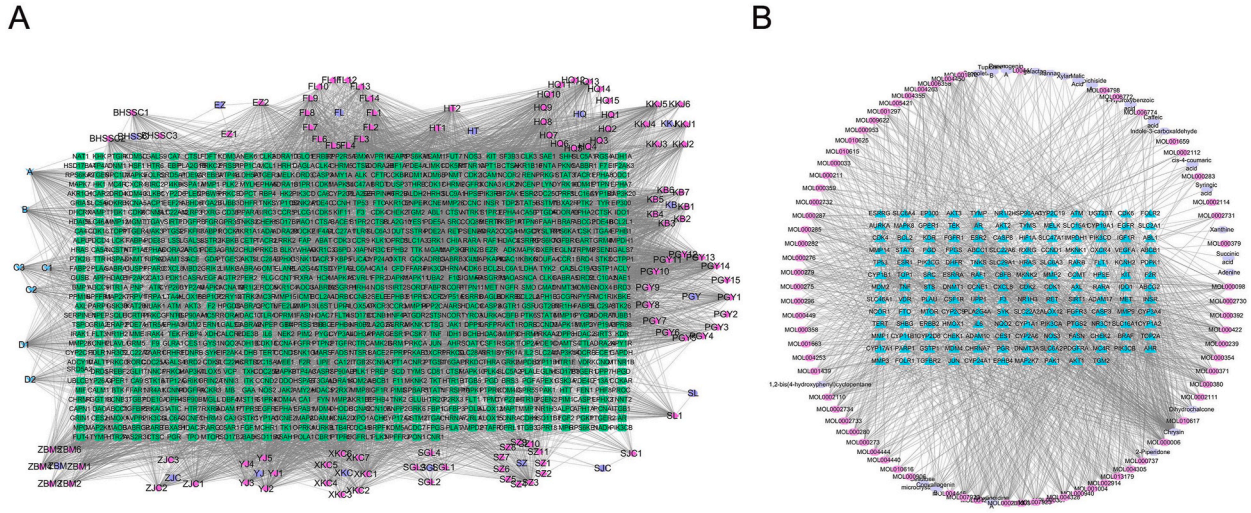

Fig. 4. (A) In the "herb-component-target" network, the purple circle represents 16 herbs, the rose red diamond represents drug active components, the blue arrow represents intersecting components, and the green rectangle represents related targets. (B) The "drug-target-disease" network includes 16 herbs, 94 active ingredients and 154 target genes. The rose red circle represents the main components of 12 herbs searched in the TCMSP, and the purple circle represents 23 active components of 4 herbs with a literature search. The blue triangle represents the disease-related target genes.

3.3. PPI network construction and key targets

To demonstrate the intersection of targets between TNBC and YAFZF, a Venn diagram of 154 intersecting targets was constructed (Fig. 5A). To identify the crucial protein of YAFZF treating TNBC, 154 intersecting targets were imported into the STRING network platform. After removing the free targets, the PPI network had 153 nodes and 2327 edges, with an average node degree of 30.4 and an average local clustering coefficient of 0.616, $P < 1.0e\text{-}16$(Fig. 5B). Due to the close connection between intersecting targets, a network was formed (Table 4). A topology analysis was performed on the PPI network using Cytoscape 3.7.2 software. The top 20 targets were filtered based on their high degree values, including tumour protein p53 (TP53), protein kinase B (AKT)1, estrogen receptor 1(ESR1), epidermal growth factor receptor (EGFR), proto-oncogene tyrosine-protein kinase Src (SRC), HRas proto-oncogene GTPase (HRAS), vascular endothelial growth factor A (VEGFA), cyclin D1 (CCND1), Jun proto-oncogene (JUN), receptor tyrosine-protein kinase erbB-2 (ERBB2), signal transducer and activator of transcription 3 (STAT3), heat shock protein HSP 90-alpha (HSP90AA1), interleukin-6 (IL6), CASP3, hypoxia-inducible factor 1 (HIF1)A, tumour necrosis factor (TNF), serine-threonine protein kinase (MTOR), phosphatidylinositol 4,5-bisphosphate 3-kinase catalytic subunit alpha isoform (PIK3CA), sirtuin 1 (SIRT1) and androgen receptor (AR), which were closely associated with TNBC(Fig. 5C).

3.4. Functional enrichment detection

To detect functional enrichment in TNBC, biological processes underlying the therapeutic effects of YAFZF were investigated. The GO analysis includes three components, biological process (BP), cellular component (CC), and molecular function (MF), which describe the functions of gene products together. A total of 153 intersecting targets were associated with 1728 BPs, 79 CCs, and 169 MFs. As shown in Fig. 5D, we selected the top 20 representative enrichment clusters based on $P < 0.01$, gene number ≥ 3 and enrichment factor >1.5. In GO analysis, BP was mainly enriched in positive regulation of cell migration, protein phosphorylation,

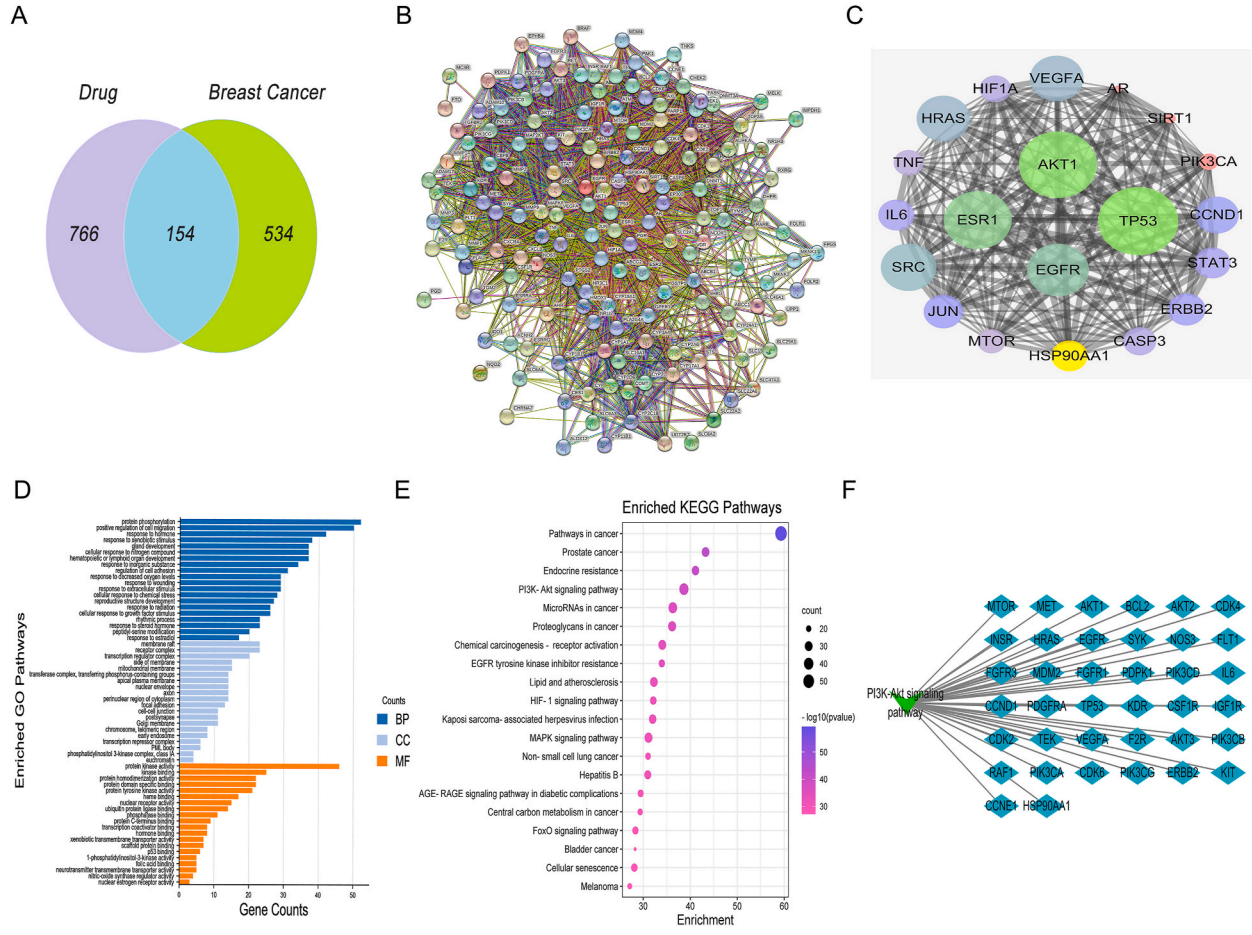

Fig. 5. Network pharmacology analysis results of YAFZF. (A) The Venn diagram shows the intersecting targets of YAFZF and TNBC. (B) The protein-protein intersection network of YAFZF and TNBC consists of 153 nodes and 2327 edges. (C) The top 20 core target genes of YAFZF in the treatment of TNBC. The node size depends on the degree values of potential targets. (D–E) GO (BP, CC, and MF) and KEGG functional enrichment detection. (F) The targets of YAFZF enriched in the PI3K/Akt pathway against TNBC.

Table 4
Top 20 hub genes information.

Gene Symbol	Degree	Betweenness Centrality	Closeness Centrality
TP53	99	0.048	0.734
AKT1	98	0.063	0.731
ESR1	93	0.057	0.707
EGFR	90	0.037	0.697
SRC	87	0.033	0.694
HRAS	86	0.029	0.682
VEGFA	86	0.026	0.691
CCND1	81	0.020	0.676
JUN	79	0.018	0.670
ERBB2	78	0.022	0.661
STAT3	77	0.040	0.664
HSP90AA1	77	0.019	0.661
IL6	77	0.023	0.664
CASP3	75	0.014	0.658
HIF1A	74	0.017	0.650
TNF	73	0.018	0.652
MTOR	72	0.026	0.641
PIK3CA	66	0.009	0.610
SIRT1	61	0.009	0.606
AR	59	0.010	0.608

reaction to xenobiotic stimulus, gland development, response to hormones, *etc*. CC in GO analysis was primarily composed of membrane raft, receptor complex, transcription regulator complex, mitochondrial membrane, transferase complex, transferring phosphorus-containing groups, *etc*. Furthermore, MF in GO analysis was mainly enriched in protein kinase activity, kinase binding, protein homodimerization activity, protein domain-specific binding, protein tyrosine kinase activity, heme binding, *etc*.

The KEGG analysis was conducted to explore the representative pathways of YAFZF treating TNBC. A total of 179 pathways were acquired from KEGG enrichment, and 20 representative KEGG pathways were screened according to $P < 0.01$, gene number ≥ 3 and enrichment factor >1.5. The 20 key KEGG pathways were made up of 5 signalling pathways related to TNBC onset and progression: pathways in cancer, PI3K-Akt signalling pathway, HIF-1 signalling pathway, mitogen-activated protein kinases (MAPK) signalling pathway and forkhead box O (FoxO) signalling pathway; 11 disease pathways unrelated to TNBC, such as microRNA in cancer, proteoglycan in cancer, central carbon metabolism in cancer, endocrine resistance, chemical carcinogenesis-receptor activation, EGFR tyrosine kinase inhibitor resistance, lipid and atherosclerosis, Kaposi's sarcoma-associated herpesvirus infection, hepatitis B, advanced

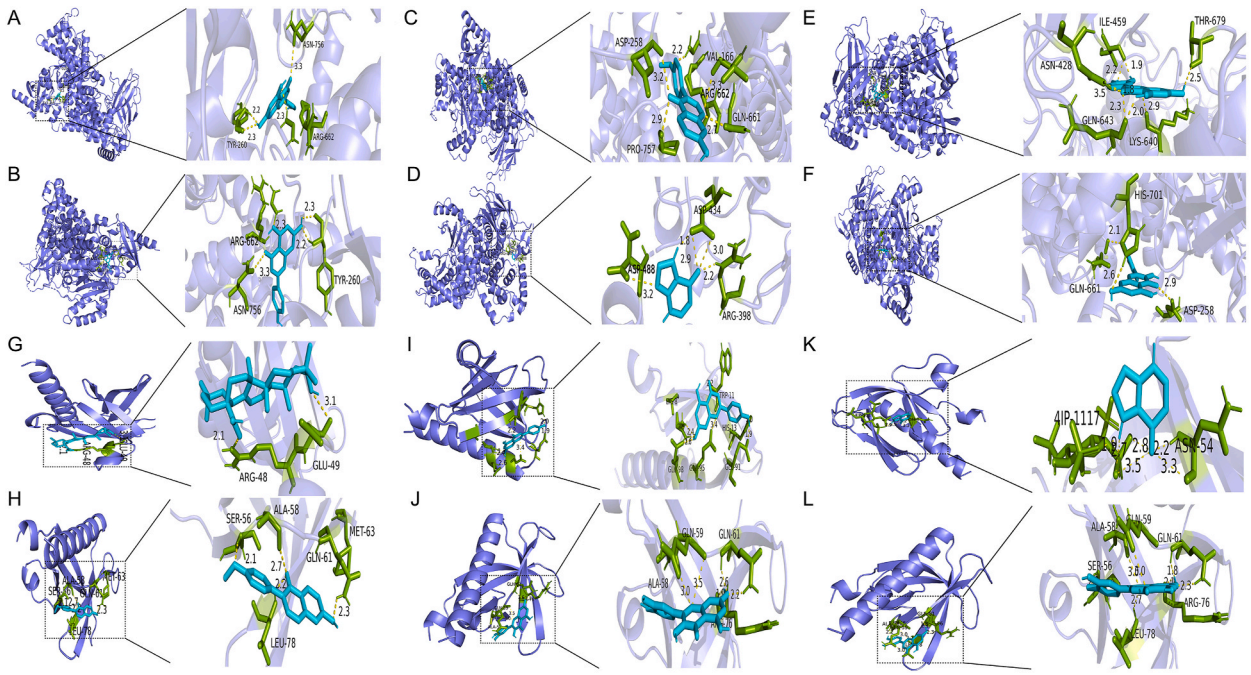

Fig. 6. The docking results of PIK3CA and AKT1 with oleanolic acid (A, G), formononetin (B, H), apigenin (C, I), quercetin (D, J), hypoxanthine (E, K) and luteolin (F, L), respectively.

glycation end products(AGE)-receptor for AGE signalling pathway in diabetic complications, cellular senescence; 4 other carcinomas, namely prostate cancer, non-small cell lung cancer, bladder cancer and melanoma (Fig. 5E). In total, 153 intersecting target genes were enriched in PI3K-Akt, HIF-1, MAPK and FoxO pathways, suggesting that YAFZF may exert therapeutic effects on TNBC by acting on multiple targets within multiple signalling pathways. According to enrichment analyses, the PI3K-Akt pathway had a higher biological significance based on the *P* value. A "target-pathway" network involving enriched target genes and the PI3K-Akt pathway was constructed to assess YAFZF's effectiveness against TNBC (Fig. 5F).

3.5. Molecular docking

Binding energies < -5.00 kcal/mol and <−7.00 kcal/mol indicate good binding and satisfactory binding effects, respectively. The six core active molecules were oleanolic acid, formononetin, apigenin, quercetin, hypoxanthine and luteolin. As shown in Fig. 6, the six core active molecules were docked and evaluated with PIK3CA and AKT1, respectively. In terms of the docking results, the six core active components formed hydrogen bonds with PIK3CA and AKT1, with a strong binding energy, as shown in Table 5.

3.6. Effects of YAFZF on TNBC cells viability, invasion and migration in vitro

To detect the effect of YAFZF on 4T1 and MDA-MB-231 cells, the cell viability and inhibition rate of 4T1 and MDA-MB-231 cells treated with different concentrations of YAFZF treatment were evaluated by CCK-8 (Fig. 7A–D**)**. The results indicated that YAFZF exposure markedly suppressed TNBC cell line 4T1 and MDA-MB-231 viability. The IC50 values of 4T1 cells at 24 h and 48 h were 31.07 and 24.13 mg/ml, while those of MDA-MB-231 cells were 31.25 and 21 mg/ml, respectively. The inhibiting rates of 4T1 cells and MDA-MB-231 cells significantly increased at concentrations of 30 mg/ml of YAFZF. *In vitro* cytotoxicity of YAFZF was also evaluated against mouse fibroblasts (NIH/3T3) and normal liver cell line (NCTC 1469) in the different concentrations of 15–75 mg/ml. The IC50 values of YAFZF against NIH/3T3 and NCTC 1469 cell lines were found to be 64.36 and 62.58 mg/ml, respectively (Fig. 7E and F). Thus, even at high dose (60 mg/ml), YAFZF demonstrated little harmful effects on negative-normal cell lines.

As shown in Fig. 8A-F, pre-treatment with PI3K agonist slightly enhanced the invasion and migration abilities of 4T1 and MDA-MB-231 cells. YAFZF treatment further reduced the number of invaded and migrated cells. Collectively, these results indicated that YAFZF induced cell death, and reversed the effects of PI3K agonist 740 Y-P on the invasion and migration abilities of 4T1 and MDA-MB-231 cells, which may be associated with the downregulation of the PI3K-related pathway.

3.7. YAFZF treatment suppressed the proliferation of TNBC cells and induced their apoptosis in Balb/c mice

The treatment of breast xenograft tumour models with YAFZF was conducted in animal experiments on Balb/c mice over 14 days (Fig. 9A**)**. Different doses of treatment group mice gained varying amounts of body weight compared to the model group mice (Fig. 9B**)**. YAFZF administration suppressed xenograft tumour growth, both in terms of weight and volume. YAFZF-44.28 g/kg group reduced tumour weights and volumes significantly compared with untreated groups, while YAFZF-22.14 g/kg group only reduced xenograft tumour weights (Fig. 9C–E**)**. IHC can determine ki67 expression in BC samples, which is now considered to be a popular biomarker for the detection of cancer proliferation [36]. The IHC results of this work suggested that Ki67-positive cells were markedly reduced in tumour tissue of the YAFZF-44.28 g/kg treatment group (Fig. 9F and G**)**.

Furthermore, the TUNEL assay enables the determination of genomic DNA breakage caused by anti-cancer agents at early and late stages of apoptosis, establishing them as measures of apoptotic cell death [37]. The YAFZF-22.14 g/kg and 44.28 g/kg groups showed an increase in apoptosis cells when compared with the model group, especially the YAFZF-44.28 g/kg group (Fig. 9H and I**)**. The anti-cancer effect of YAFZF in TNBC mice was confirmed by its ability to suppress proliferation and induce apoptosis of TNBC cells.

3.8. Effects of YAFZF on TNBC metastasis through the PI3K/Akt/mTOR pathway regulating epithelial-mesenchymal transition (EMT)

EMT is linked with loss of adhesion and polarity between cells, which leads to tumour invasion, metastasis, and progression. The process of EMT is triggered by EMT-transcription factors (EMT-TFs) such as SNAIL and TWIST, which cause the conversion of epithelial cells into mesenchymal cells with reduced expression of E-cadherin and growing expression of Vimentin [38]. A large number of studies have elucidated that PI3K/Akt/mTOR is a classic signalling pathway that promotes tumour migration and metastasis by regulating EMT [39,40].

Table 5
Binding energies of molecular docking.

Components	PIK3CA	AKT1
Oleanolic acid	−8.86	−7.13
Formononetin	−7.67	−6.63
Apigenin	−6.95	−6.37
Quercetin	−6.17	−5.21
Hypoxanthine	−5.09	−5.26
Luteolin	−7.34	−6.02

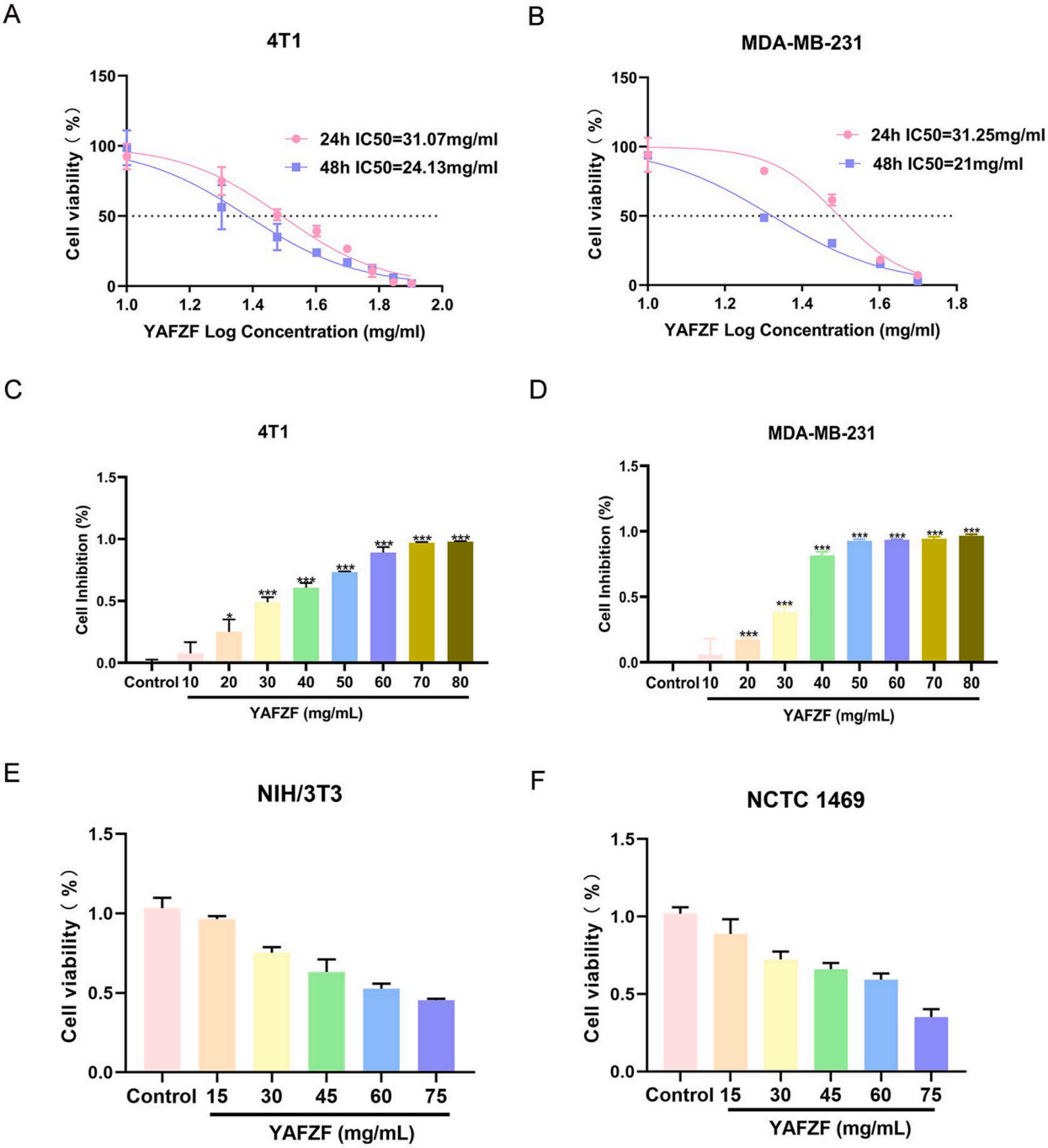

Fig. 7. (A–B) IC50 values of 4T1 and MDA-MB-231 cells after YAFZF administration for 24 h and 48 h. (C–D) Cell inhibition rates of 4T1 and MDA-MB-231 cells under different concentrations of YAFZF treatment (24 h). (E–F) Cytotoxic activity of YAFZF treatment (24 h) against mouse fibroblasts (NIH/3T3) and normal liver cell (NCTC 1469). Data were expressed as mean ± SD, $^{*}P < 0.05$, $^{***}P < 0.001$ vs. control group.

Our study found that the PI3K/Akt/mTOR pathway inhibition was observed after YAFZF administration at different doses (Fig. 10A–D**)**. To examine the effects of YAFZF on TNBC metastasis, qRT-PCR and WB methods were used to examine mRNA levels and protein expressions of EMT-TFs and related markers. YAFZF-22.14 g/kg and YAFZF-44.28 g/kg significantly suppressed mRNA levels and expressions of EMT-TFs and Vimentin, whereas E-cadherin protein expression only increased in the YAFZF-44.28 g/kg group (Fig. 10E–J**)**. After YAFZF therapy, SNAIL expression was decreased, while only the YAFZF-44.28 g/kg group had down-regulation and up-regulation of Vimentin and E-cadherin in the IHC staining (Fig. 11A–D**)**.

The lung and liver tissues of TNBC tumour models were observed for pathological changes to further investigate the therapeutic

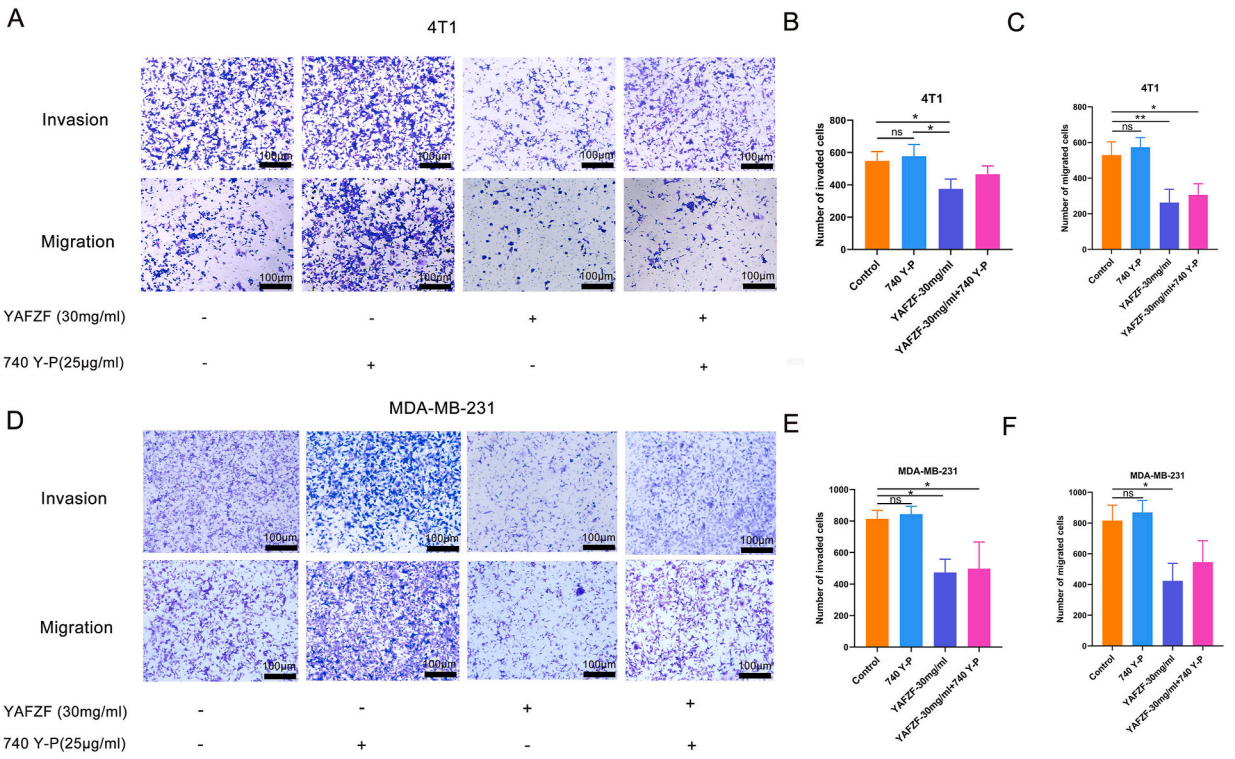

Fig. 8. (A–C) The invasion and migration images and quantitative analysis of 4T1 cells upon 740Y-P (25 μg/ml), YAFZF exposure (30 mg/ml). (D–F) The invasion and migration images and quantitative analysis of MDA-MB-231 cell upon 740Y-P (25 μg/ml), YAFZF exposure (30 mg/ml). The scale bar was 100 μm. Data were expressed as mean ± SD, $^{*}P < 0.05$, $^{**}P < 0.01$ vs. control group, ns means no statistical significance.

effects of YAFZF on TNBC metastasis. HE stained lung sections of mice bearing breast xenograft tumours showed several tumour metastatic areas and severe destruction of their lungs. In contrast, after YAFZF intervention, tumour metastatic areas significantly diminished, and these pulmonary tissues recovered to normal morphology. A significant decrease in the ratio of TNBC lung metastasis was also observed after administering YAFZF-44.28 g/kg over the model and YAFZF-11.07 g/kg groups (Fig. 11E and F). Liver-stained tissues of mice with 4T1 xenograft tumours showed fragmented hepatic lobes and dense tumour metastatic lesions. YAFZF intervention significantly reduced the ratio of these metastatic areas, especially in the YAFZF-44.28 g/kg group (Fig. 11G and H). Thus, YAFZF may inhibit TNBC metastasis by the PI3K/Akt/mTOR pathway regulating EMT.

4. Discussion

Several factors are involved in the progression of TNBC biology, including low socioeconomic status, limited access to healthcare, complex genetic architecture, imbalanced body's internal environment, and negative lifestyle [23,41]. Natural medicine and TCM have been used postoperatively and adjuvantly for carcinomas owing to their low toxicity, anti-cancer properties, and unique pharmacological properties. In light of the compatibility of KYP and several clinical experiences with TNBC treatment, YAFZF has been built and verified to improve spleen function, strengthen Qi, resolve phlegm and remove blood stasis, remove heat and detoxify, and maintain the body's internal environment in a homeostasis state. The apparent efficacy of YAFZF in TNBC patients with regard to alleviating their pain, prolonging their survival period, and improving their quality of life was verified in clinical practice. However, the deep mechanism by which YAFZF fights TNBC remains unclear. In the present study, TNBC was successfully treated using YAFZF, which effectively inhibited cell proliferation, induced apoptosis, caused cell death and reduced the invasion, migration and metastasis potential of tumour cells. In particular, it appears that the anti-invasion, anti-migration and anti-metastasis potential of YAFZF is influenced by the PI3K/Akt/mTOR pathway modulating EMT (Fig. 12).

To explore the bioactive components of YAFZF, UPLC-Q-Orbitrap-HRMS analysis was conducted. The following components of YAFZF were found to have bioactive properties in treating TNBC: oleanolic acid, formononetin, apigenin, quercetin, hypoxanthine, and luteolin. Oleanolic acid is a pentacyclic triterpenoid originating from plants, which is low toxic and has anti-cancer properties, making chemotherapy and radiation therapy more effective [42]. A study demonstrated that oleanolic acid suppresses BC cell growth and induces apoptosis to treat BC [43]. Formononetin, an isoflavone, has shown therapeutic potential in various diseases, including neurodegenerative diseases, metabolic syndrome, and cancer. The effects of formononetin on tumour cell cycle, proliferation, and even apoptosis may make it a promising anti-cancer agent [44]. Due to its low toxicity, apigenin, a flavonoid enhances the immune system and has antioxidant, antiviral, and anti-cancer properties. The presence of apigenin sensitizes TNBC spheroids to doxorubicin-induced

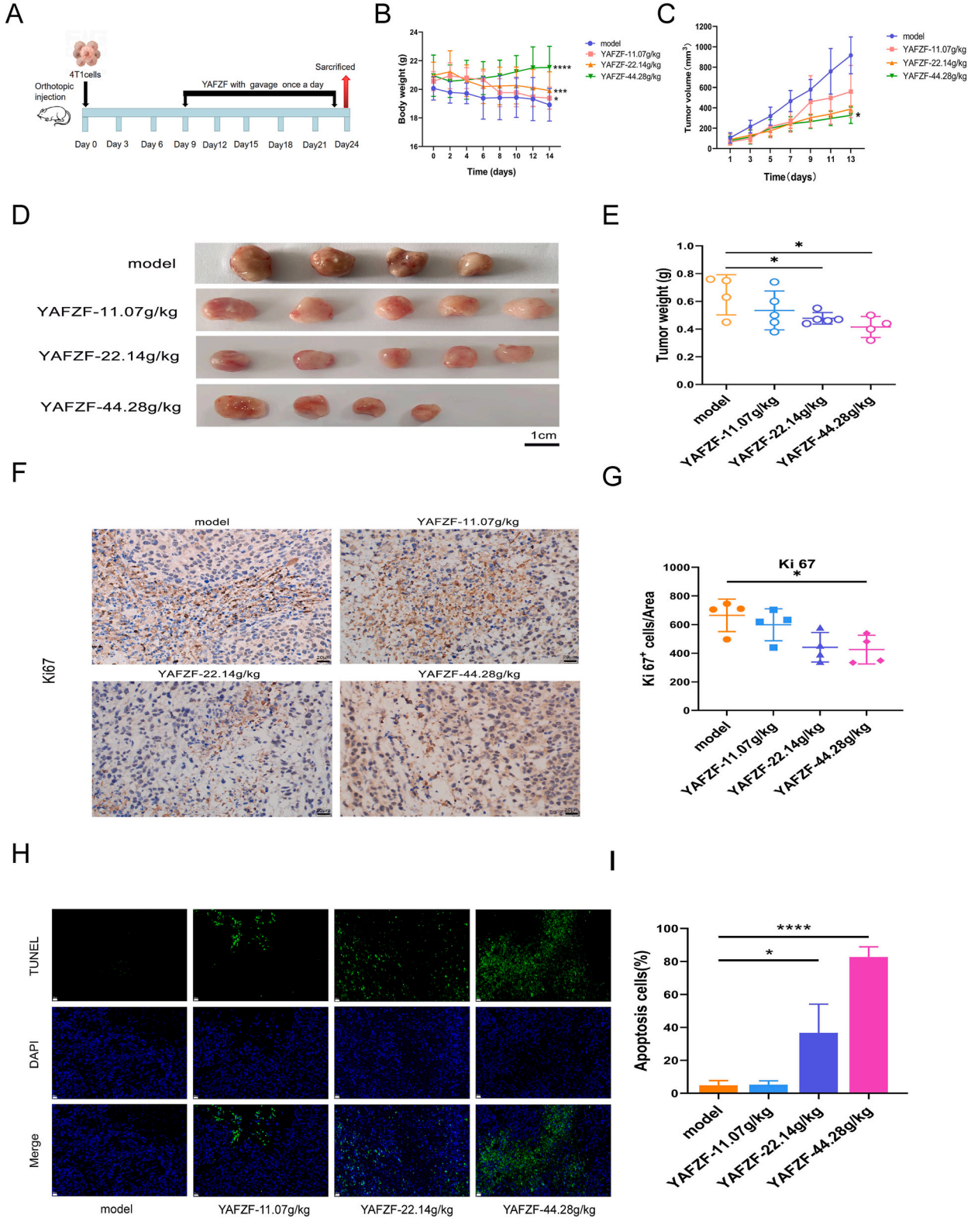

(caption on next page)

Fig. 9. YAFZF suppressed proliferation and induced apoptosis of cancer cells in xenograft tumour models. (A) Flow diagram of the animal experiment. (B) The weight changes in TNBC mice treated with YAFZF (11.07, 22.14 and 44.28 g/kg). (C–E) Tumour volume and weight changes after YAFZF interventions of 11.07, 22.14 and 44.28 g/kg (F–G) Representative IHC images of tumour proliferation and quantification of Ki67 expression (magnification: ×400; scale bar:20 μm). (H-I) Representative images of TUNEL staining and apoptosis-positive cells were calculated (magnification: ×400; scale bar: 20 μm). Data were expressed as mean ± SD, $^{*}P < 0.05$, $^{***}P < 0.001$, $^{****}P < 0.0001$vs. model group.

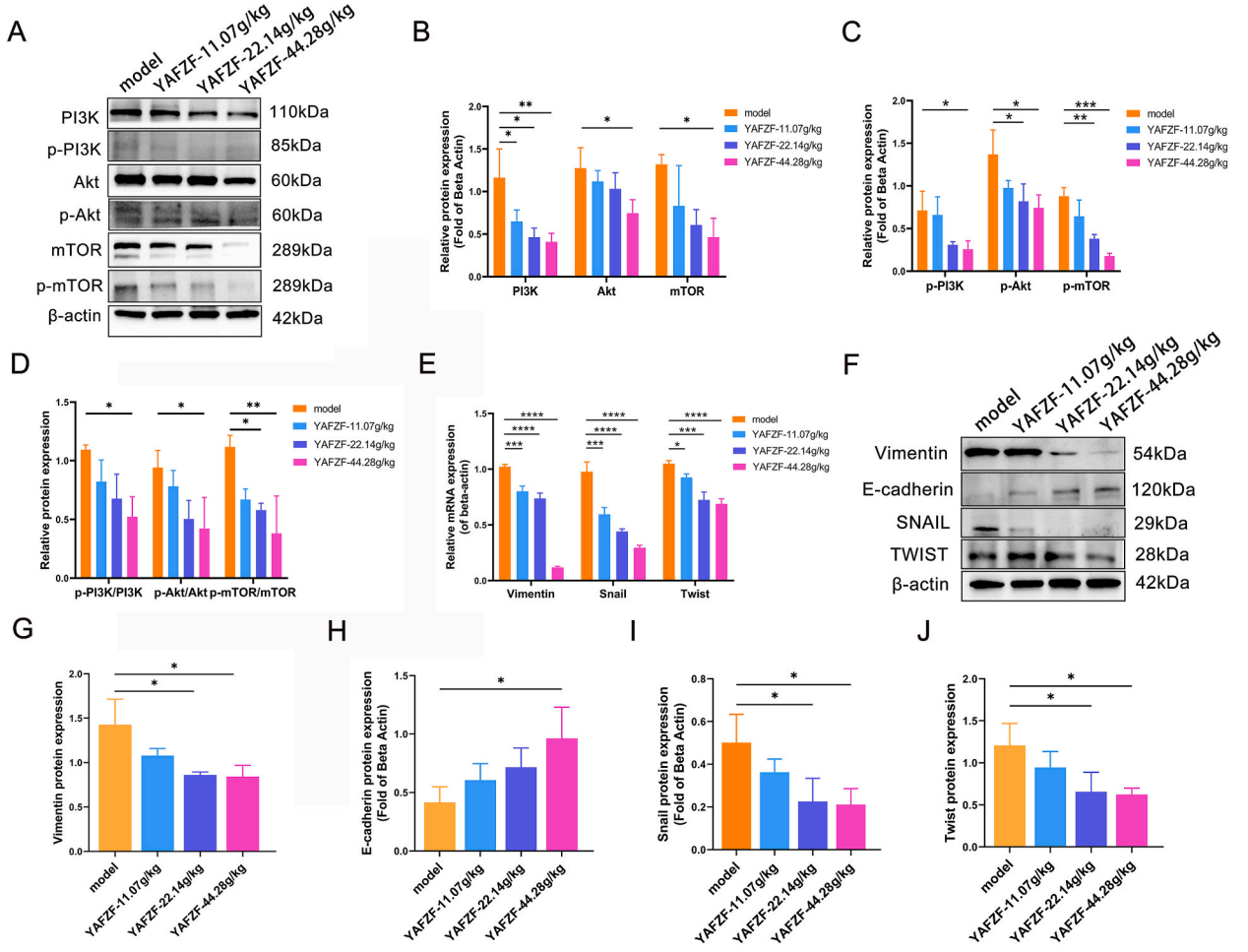

Fig. 10. (A–D) Related protein expressions were detected by WB in the PI3K/Akt/mTOR pathway. (E–J) mRNA levels and protein expressions of EMT-TFs and related markers were detected in xenograft tumour tissues. Data were expressed as mean ± SD, $^{*}P < 0.05$, $^{**}P < 0.01$, $^{***}P < 0.001$, $^{****}P < 0.0001$vs. model group. All of the original, non-adjusted blot images for A and F were provided in supplementary material.

apoptosis through heterogeneous ribonuclear protein A2/B1 (HnRNPA2), emphasizing its importance in chemotherapy [45]. Flavonoids such as quercetin are beneficial to cancer cells, which may lower BC risk. Quercetin provides anti-cancer properties for BC treatment, including antioxidant, anti-inflammation, apoptosis, growth inhibition, and angiogenesis inhibition [46]. In experimental studies, the antioxidant properties of flavonoids, like luteolin, appear to benefit cancer cells [47]. In a previous study, luteolin reduced matrix metalloproteinase (MMP) 9 levels through the AKT/mTOR pathway, inhibiting the proliferation and metastasis of androgen receptor-positive TNBC [48]. Overall, these YAFZF active components exert their unique anti-cancer properties through various mechanisms, making them promising candidates for treating TNBC.

The action mechanism of YAFZF treating TNBC is further demonstrated through network pharmacological analysis and molecular docking. Based on the "component-target-pathway" regulatory interaction network construction of network pharmacology [49], we screened 153 YAFZF potential targets affecting TNBC, and of those, TP53, AKT1, ESR1, EGFR, SRC and VEGFA may play a crucial role. TP53 gene mutations are frequent in cancer, including BC, and contribute to its pathogenesis [50]. Due to its excessive activation of stimulated signals and its role in cell-cycle arrest, DNA repair, *etc.*, TP53 is considered an important symbol in cancer biology [51]. Activated AKT protein kinases are secreted into the nucleus and catalyze several substrates that regulate various cell functions, including metabolism, survival, angiogenesis, migration, invasion, and more [52]. Mutations in AKT1 are strongly related to BC onset for its important role in cell proliferation and metastasis. The ESR1 mutations exhibit a distinctive transcriptional profile, easily

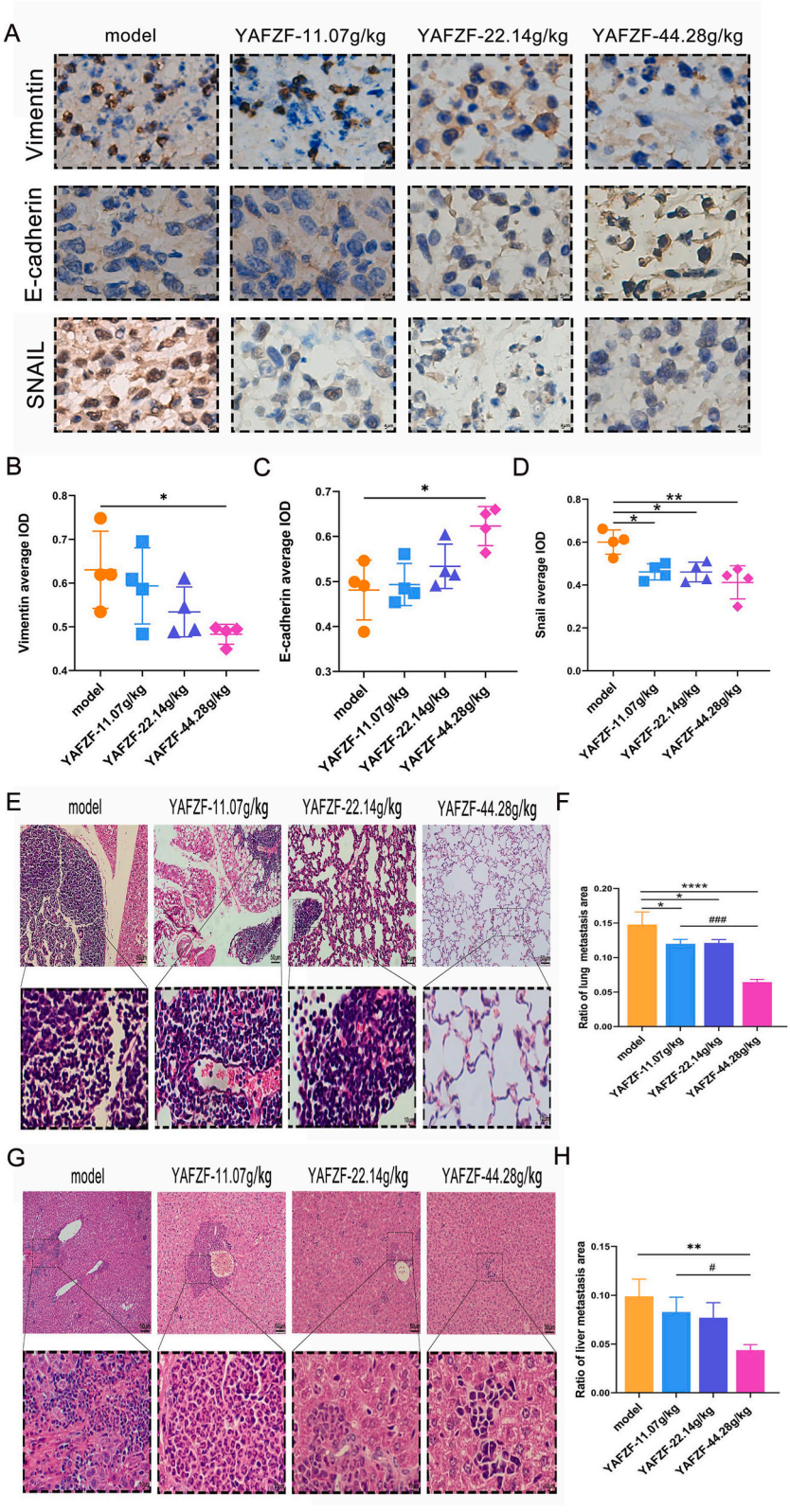

(caption on next page)

Fig. 11. (A–D) Representative images and expression levels of Vimentin, E-cadherin and SNAIL were detected in tumour tissue sections by IHC staining; the scale bar was 4 μm.(E–F) Representative images and semi-quantitative analysis of lung metastatic areas in HE staining of TNBC mice models. Scale bars were 50 and 10 μm, respectively. (G–H) Representative images and semi-quantitative analysis of liver metastatic areas in HE staining of TNBC mice models. Scale bars were 50 and 10 μm, respectively. Data were expressed as mean ± SD, $^{*}P < 0.05$, $^{**}P < 0.01$, $^{****}P < 0.0001$vs. model group; $^{\#}P < 0.05$, $^{\#\#\#}P < 0.001$ vs. YAFZF-11.07 g/kg group.

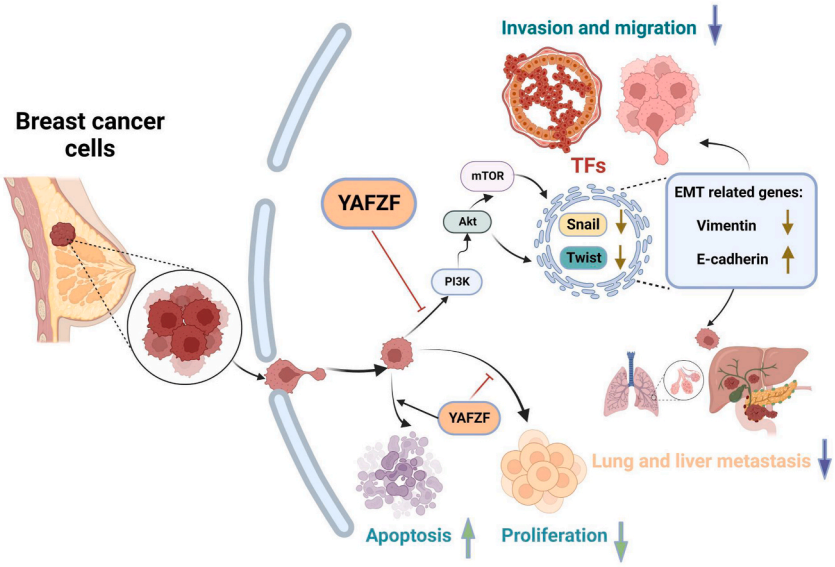

Fig. 12. Anti-cancer mechanism of YAFZF on TNBC through pathway suppression and alteration in tumour cell numbers.

enriched during tumour metastasis. This mutation resulted in constitutive transcriptional activity and decreased endocrine therapy sensitivity, leading to therapeutic resistance and BC recurrence [53]. As a member of the HER family, EGFR promotes cancer metastasis and worse prognoses. Due to its altered effect on cell growth and motility, EGFR is an ideal target for treating TNBC due to its high expression in the disease [54]. The SRC regulates several cell activities that influence tumourigenesis, progression, and prognosis in BC. The activity of SRC-induced phosphorylation is associated with cell adhesion and even metastasis of BC, which makes SRC inhibitors excellent candidates for treating this disorder [55]. The up-regulation of VEGFA in hypoxic environments triggers tumour angiogenesis due to cell proliferation and migration, vascular permeability, and endothelium inflammation [56]. These targeted genes were closely associated with tumour proliferation, migration and metastasis. These tumour-related genes might be targeted by YAFZF to exert therapeutic effects, further influencing TNBC.

Based on GO and KEGG functional analyses, YAFZF inhibiting TNBC primarily affected cell migration, protein phosphorylation, protein kinase activity, protein homodimerization activity, protein tyrosine kinase activity and heme binding, as well as several signalling pathways: PI3K-Akt, HIF-1, MAPK and FoxO pathway. PI3K-Akt is the pathway enriched with the most targeted genes, making it the main pathway of YAFZF that affects TNBC. The PI3K family of three lipid kinases regulates various biological functions in cells. In response to stimulation of PIK3CA, phosphatidylinositol (4,5)-bisphosphate (PIP2) and phosphatidylinositol (3,4,5)-triphosphate (PIP3) are produced, which activate AKT and the mTOR complex. EMT and tumour cell metastasis are mediated by the mTOR kinase, one of the downstream proteins of Akt. EMT is accelerated in BC when PIK3CA is activated, increasing the ability of tumour cells to metastasize [57]. TNBC invasion and metastasis can be inhibited by several active components found in plants and their extracts that regulate the EMT process and the PI3K/Akt/mTOR pathway [58,59]. Our study identified six YAFZF active components that bind strongly to proteins in the PI3K/Akt pathway. YAFZF significantly induced cell death and exerted inhibitory effects on the invasion and migration capacities of 4T1 cells, potentially through the modulation of the PI3K/Akt/mTOR signalling pathway. Additionally, YAFZF treatment decreased the expressions of the PI3K/Akt/mTOR pathway and the levels of Vimentin, SNAIL, and TWIST while enhancing E-cadherin expression. Furthermore, YAFZF reduced lung and liver metastases in TNBC mice models. Therefore, it is possible that YAFZF could exert a significant inhibitory effect on tumour cell invasion and migration, and xenograft tumour metastasis by modulating the PI3K/Akt/mTOR pathway to treat TNBC. This mechanism of action may be associated with the regulation of the EMT program.

The processes of proliferation and apoptosis are crucial to tumourigenesis and tumour development. Resveratrol, a natural substance, inhibited the proliferation of BC cells by slowing tumour growth and triggering apoptosis in 4T1 cells in a dose- and time-related manner [60]. In our study, the decrease in weights and volumes of xenograft tumours after YAFZF treatment and the reduction of Ki67 expression in mice expressing TNBC further supported the idea that YAFZF inhibited TNBC cell proliferation. A growing number of apoptosis cells were observed in xenograft tumour tissues treated with YAFZF, which indicates that YAFZF could induce

tumour cell apoptosis in TNBC. TNBC mice treated with YAFZF gained weight, suggesting that YAFZF could improve patients' clinical outcomes. Therefore, YAFZF exerts its anti-cancer effects on TNBC by suppressing proliferation and inducing apoptosis of tumour cells.

We have limited information about YAFZF's metabolite and side effects when treating TNBC. In addition to its complex active ingredients, YAFZF also targets multiple genes and signalling pathways against TNBC. Further studies are needed to investigate YAFZF's pharmacokinetics and specific targets on TNBC cells.

5. Conclusion

UPLC-Q-Orbitrap-HRMS analysis, network pharmacology, molecular docking, *in vitro and in vivo* experiments revealed how YAFZF acted against TNBC in this study. It has been demonstrated that YAFZF exhibited a significant inhibitory effect on tumour cell invasion and migration as well as xenograft tumour metastasis, which may be mediated by the PI3K/Akt/mTOR pathway and associated with EMT regulation. Furthermore, YAFZF exerted anti-cancer activity against TNBC by inducing apoptosis, leading to cell death and suppressing the proliferation of cancer cells. The findings in our study enhance the understanding of the pharmacological mechanism of YAFZF, offering new perspectives for TNBC treatment with TCM.

Ethical statement

This study was conducted in accordance with the ARRIVE guidelines and approved by Wuhan University's Zhongnan Hospital Experimental Animal Welfare Ethics Committee (Approval No. ZN2022059) on 20-03-2022.

Data availability statement

The data associated with this study will be deposited into a publicly available repository upon publication. All the data used to support this study will be made available on request.

CRediT authorship contribution statement

Ruijie Li: Writing – original draft, Validation, Software, Methodology, Investigation, Funding acquisition. **Haoliang Ke:** Supervision, Methodology, Investigation. **Pan Liu:** Validation, Supervision, Investigation. **Qian Yang:** Validation, Investigation. **Yuxin Li:** Validation, Software, Investigation. **Longzhu Ke:** Investigation. **Xiuping Wang:** Supervision, Investigation. **Chaoyan Wu:** Writing – review & editing, Supervision, Conceptualization. **Yingwen Zhang:** Writing – review & editing, Supervision, Methodology, Conceptualization.

Declaration of competing interest

The authors declare that they have no known competing financial interests or personal relationships that could have appeared to influence the work reported in this paper.

Acknowledgments

This study received financial support from the provincial administration of traditional Chinese medicine in Hubei (No. ZY2023Z009).

Appendix A. Supplementary data

Supplementary data to this article can be found online at https://doi.org/10.1016/j.heliyon.2024.e36579.

References

[1] A.C. Garrido-Castro, N.U. Lin, K. Polyak, Insights into molecular classifications of triple-negative breast cancer: improving patient selection for treatment, Cancer Discov. 9 (2) (2019) 176–198, https://doi.org/10.1158/2159-8290.Cd-18-1177.

[2] I. Fatima, I. El-Ayachi, H.C. Playa, J.A. Alva-Ornelas, A.B. Khalid, W.L. Kuenzinger, P. Wend, J.C. Pence, L. Brakefield, R.I. Krutilina, D.L. Johnson, R. M. O'Regan, V. Seewaldt, T.N. Seagroves, S.A. Krum, G.A. Miranda-Carboni, Simultaneous multi-organ metastases from chemo-resistant triple-negative breast cancer are prevented by interfering with WNT-signaling, Cancers 11 (12) (2019), https://doi.org/10.3390/cancers11122039.

[3] R. Islam, K.W. Lam, Recent progress in small molecule agents for the targeted therapy of triple-negative breast cancer, Eur. J. Med. Chem. 207 (2020) 112812, https://doi.org/10.1016/j.ejmech.2020.112812.

[4] P. Zhao, Y. Xu, W. Ji, S. Zhou, L. Li, L. Qiu, Z. Qian, X. Wang, H. Zhang, Biomimetic black phosphorus quantum dots-based photothermal therapy combined with anti-PD-L1 treatment inhibits recurrence and metastasis in triple-negative breast cancer, J. Nanobiotechnol. 19 (1) (2021) 181, https://doi.org/10.1186/s12951-021-00932-2.

[5] S. Wang, J.L. Fu, H.F. Hao, Y.N. Jiao, P.P. Li, S.Y. Han, Metabolic reprogramming by traditional Chinese medicine and its role in effective cancer therapy, Pharmacol. Res. 170 (2021) 105728, https://doi.org/10.1016/j.phrs.2021.105728.

[6] Wenshao He, Observation on the curative effect of Kaiyu powder modified treatment on 78 cases of breast hyperplasia, New Chinese Medicine 44 (10) (2012) 53–54.

[7] A. Sheik, K. Kim, G.L. Varaprasad, H. Lee, S. Kim, E. Kim, J.Y. Shin, S.Y. Oh, Y.S. Huh, The anti-cancerous activity of adaptogenic herb Astragalus membranaceus, Phytomedicine 91 (2021) 153698, https://doi.org/10.1016/j.phymed.2021.153698.

[8] Z. Wang, J. Xu, Y. Wang, L. Xiang, X. He, Total saponins from Tupistra chinensis baker inhibits growth of human gastric cancer cells in vitro and in vivo, J. Ethnopharmacol. 278 (2021) 114323, https://doi.org/10.1016/j.jep.2021.114323.

[9] J. Jia, X. Li, X. Ren, X. Liu, Y. Wang, Y. Dong, X. Wang, S. Sun, X. Xu, X. Li, R. Song, J. Ma, A. Yu, Q. Fan, J. Wei, X. Yan, X. Wang, G. She, Sparganii Rhizoma: a review of traditional clinical application, processing, phytochemistry, pharmacology, and toxicity, J. Ethnopharmacol. 268 (2021) 113571, https://doi.org/10.1016/j.jep.2020.113571.

[10] M.H. Wang, M. Long, B.Y. Zhu, S.H. Yang, J.H. Ren, H.Z. Zhang, Effects of sargentgloryvine stem extracts on HepG-2 cells in vitro and in vivo, World J. Gastroenterol. 17 (23) (2011) 2848–2854, https://doi.org/10.3748/wjg.v17.i23.2848.

[11] Z. Zhou, Y. Peng, W. Ai, Q. Li, T. Ye, C. Wu, H. Ke, X. Wang, Y. Zhang, Compound Opening Arrow Mixture exerts anti-tumor effects in a mouse model of breast cancer, Sci. Rep. 10 (1) (2020) 8175, https://doi.org/10.1038/s41598-020-64561-9.

[12] C. Nogales, Z.M. Mamdouh, M. List, C. Kiel, A.I. Casas, Hhhw Schmidt, Network pharmacology: curing causal mechanisms instead of treating symptoms, Trends Pharmacol. Sci. 43 (2) (2022) 136–150, https://doi.org/10.1016/j.tips.2021.11.004.

[13] X. Wang, Z.Y. Wang, J.H. Zheng, S. Li, TCM network pharmacology: a new trend towards combining computational, experimental and clinical approaches, Chin. J. Nat. Med. 19 (1) (2021) 1–11, https://doi.org/10.1016/S1875-5364(21)60001-8.

[14] L. Zhao, H. Zhang, N. Li, J. Chen, H. Xu, Y. Wang, Q. Liang, Network pharmacology, a promising approach to reveal the pharmacology mechanism of Chinese medicine formula, J. Ethnopharmacol. 309 (2023) 116306, https://doi.org/10.1016/j.jep.2023.116306.

[15] Y.H. Li, C.Y. Yu, X.X. Li, P. Zhang, J. Tang, Q. Yang, T. Fu, X. Zhang, X. Cui, G. Tu, Y. Zhang, S. Li, F. Yang, Q. Sun, C. Qin, X. Zeng, Z. Chen, Y.Z. Chen, F. Zhu, Therapeutic target database update 2018: enriched resource for facilitating bench-to-clinic research of targeted therapeutics, Nucleic Acids Res. 46 (D1) (2018) D1121–d1127, https://doi.org/10.1093/nar/gkx1076.

[16] J. Ru, P. Li, J. Wang, W. Zhou, B. Li, C. Huang, P. Li, Z. Guo, W. Tao, Y. Yang, X. Xu, Y. Li, Y. Wang, L. Yang, TCMSP: a database of systems pharmacology for drug discovery from herbal medicines, J. Cheminf. 6 (2014) 13, https://doi.org/10.1186/1758-2946-6-13.

[17] A. Daina, O. Michielin, V. Zoete, SwissADME: a free web tool to evaluate pharmacokinetics, drug-likeness and medicinal chemistry friendliness of small molecules, Sci. Rep. 7 (2017) 42717, https://doi.org/10.1038/srep42717.

[18] A. Daina, O. Michielin, V. Zoete, SwissTargetPrediction: updated data and new features for efficient prediction of protein targets of small molecules, Nucleic Acids Res. 47 (W1) (2019) W357–w364, https://doi.org/10.1093/nar/gkz382.

[19] UniProt: a worldwide hub of protein knowledge, Nucleic Acids Res. 47 (D1) (2019) D506–d515, https://doi.org/10.1093/nar/gky1049.

[20] G. Stelzer, I. Dalah, T.I. Stein, Y. Satanower, N. Rosen, N. Nativ, D. Oz-Levi, T. Olender, F. Belinky, I. Bahir, H. Krug, P. Perco, B. Mayer, E. Kolker, M. Safran, D. Lancet, In-silico human genomics with GeneCards, Hum. Genom. 5 (6) (2011) 709–717, https://doi.org/10.1186/1479-7364-5-6-709.

[21] J.M. Barbarino, M. Whirl-Carrillo, R.B. Altman, T.E. Klein, PharmGKB: a worldwide resource for pharmacogenomic information, Wiley interdisciplinary reviews. Systems biology and medicine 10 (4) (2018) e1417, https://doi.org/10.1002/wsbm.1417.

[22] J.S. Amberger, C.A. Bocchini, F. Schiettecatte, A.F. Scott, A. Hamosh, OMIM.org: online Mendelian Inheritance in Man (OMIM®), an online catalog of human genes and genetic disorders, Nucleic Acids Res. 43 (Database issue) (2015) D789–D798, https://doi.org/10.1093/nar/gku1205.

[23] O. Prakash, F. Hossain, D. Danos, A. Lassak, R. Scribner, L. Miele, Racial disparities in triple negative breast cancer: a review of the role of biologic and non-biologic factors, Front. Public Health 8 (2020) 576964, https://doi.org/10.3389/fpubh.2020.576964.

[24] J. Piñero, J.M. Ramírez-Anguita, J. Saüch-Pitarch, F. Ronzano, E. Centeno, F. Sanz, L.I. Furlong, The DisGeNET knowledge platform for disease genomics: 2019 update, Nucleic Acids Res. 48 (D1) (2020) D845–d855, https://doi.org/10.1093/nar/gkz1021.

[25] D. Szklarczyk, J.H. Morris, H. Cook, M. Kuhn, S. Wyder, M. Simonovic, A. Santos, N.T. Doncheva, A. Roth, P. Bork, L.J. Jensen, C. von Mering, The STRING database in 2017: quality-controlled protein-protein association networks, made broadly accessible, Nucleic Acids Res. 45 (D1) (2017) D362–d368, https://doi.org/10.1093/nar/gkw937.

[26] Y. Zhou, B. Zhou, L. Pache, M. Chang, A.H. Khodabakhshi, O. Tanaseichuk, C. Benner, S.K. Chanda, Metascape provides a biologist-oriented resource for the analysis of systems-level datasets, Nat. Commun. 10 (1) (2019) 1523, https://doi.org/10.1038/s41467-019-09234-6.

[27] W. Luo, C. Brouwer, Pathview: an R/Bioconductor package for pathway-based data integration and visualization, Bioinformatics 29 (14) (2013) 1830–1831, https://doi.org/10.1093/bioinformatics/btt285.

[28] S. Kim, J. Chen, T. Cheng, A. Gindulyte, J. He, S. He, Q. Li, B.A. Shoemaker, P.A. Thiessen, B. Yu, L. Zaslavsky, J. Zhang, E.E. Bolton, PubChem in 2021: new data content and improved web interfaces, Nucleic Acids Res. 49 (D1) (2021) D1388–d1395, https://doi.org/10.1093/nar/gkaa971.

[29] S.K. Burley, H.M. Berman, G.J. Kleywegt, J.L. Markley, H. Nakamura, S. Velankar, Protein Data Bank (PDB): the single global macromolecular structure archive, Methods Mol. Biol. 1607 (2017) 627–641, https://doi.org/10.1007/978-1-4939-7000-1_26.

[30] Litian Ma Canjun Zhao, Xinjie Wang, Wan Liu, Zhicheng Li, Aoyu Shi, Jin Zheng Liquid chromatography-mass spectrometry analysis and identification of the components contained in the new method egg oil of the hospital preparations, Modern Oncology 28 (11) (2020) 1815–1820.

[31] Xu A-lei, Oleanolic Acid Combined with Olaparib Enhances Radiosensitization in Triple Negative Breast Cancer and Imaging with ^{18}F-FETNIM Micro PET, CT Anhui Medical University, 2023.

[32] M. Xin, Y. Wang, Q. Ren, Y. Guo, Formononetin and metformin act synergistically to inhibit growth of MCF-7 breast cancer cells in vitro, Biomed. Pharmacother. 109 (2019) 2084–2089, https://doi.org/10.1016/j.biopha.2018.09.033.

[33] Xu Jian, Effect and Mechanism of Apigenin on Triple-Negative Breast Cancer, Guangzhou University of Chinese Medicine, 2019.

[34] P. Zhang, J. Zhang, L. Zhao, S. Li, K. Li, Quercetin attenuates the cardiotoxicity of doxorubicin-cyclophosphamide regimen and potentiates its chemotherapeutic effect against triple-negative breast cancer, Phytother Res. : PT 36 (1) (2022) 551–561, https://doi.org/10.1002/ptr.7342.

[35] Dai Cao, Effect and Mechanism of Luteolin on Suppressing Triple-Negative Breast Cancer, Guangzhou University of Chinese Medicine, 2021.

[36] F. Penault-Llorca, N. Radosevic-Robin, Ki67 assessment in breast cancer: an update, Pathology 49 (2) (2017) 166–171, https://doi.org/10.1016/j.pathol.2016.11.006.

[37] R. Mirzayans, D. Murray, Do TUNEL and other apoptosis assays detect cell death in preclinical studies? Int. J. Mol. Sci. 21 (23) (2020) https://doi.org/10.3390/ijms21239090.

[38] T. Brabletz, R. Kalluri, M.A. Nieto, R.A. Weinberg, EMT in cancer, Nat. Rev. Cancer 18 (2) (2018) 128–134, https://doi.org/10.1038/nrc.2017.118.

[39] Y. Li, T. Wu, Y. Wang, L. Yang, C. Hu, L. Chen, S. Wu, γ-Glutamyl cyclotransferase contributes to tumor progression in high grade serous ovarian cancer by regulating epithelial-mesenchymal transition via activating PI3K/AKT/mTOR pathway, Gynecol. Oncol. 149 (1) (2018) 163–172, https://doi.org/10.1016/j.ygyno.2018.01.023.

[40] B.T. Vo, D. Morton Jr., S. Komaragiri, A.C. Millena, C. Leath, S.A. Khan, TGF-β effects on prostate cancer cell migration and invasion are mediated by PGE2 through activation of PI3K/AKT/mTOR pathway, Endocrinology 154 (5) (2013) 1768–1779, https://doi.org/10.1210/en.2012-2074.

[41] A.M. Karim, J. Eun Kwon, T. Ali, J. Jang, I. Ullah, Y.G. Lee, D.W. Park, J. Park, J.W. Jeang, S.C. Kang, Triple-negative breast cancer: epidemiology, molecular mechanisms, and modern vaccine-based treatment strategies, Biochem. Pharmacol. 212 (2023) 115545, https://doi.org/10.1016/j.bcp.2023.115545.

[42] L. Ziberna, D. Samec, A. Mocan, S.F. Nabavi, A. Bishayee, A.A. Farooqi, A. Sureda, S.M. Nabavi, Oleanolic acid alters multiple cell signaling pathways: implication in cancer prevention and therapy, Int. J. Mol. Sci. 18 (3) (2017), https://doi.org/10.3390/ijms18030643.

[43] Z. Liang, R. Pan, X. Meng, J. Su, Y. Guo, G. Wei, Z. Zhang, K. He, Transcriptome study of oleanolic acid in the inhibition of breast tumor growth based on high-throughput sequencing, Aging 13 (19) (2021) 22883–22897, https://doi.org/10.18632/aging.203582.

[44] J. Machado Dutra, P.J.P. Espitia, R. Andrade Batista, Formononetin: biological effects and uses - a review, Food Chem. 359 (2021) 129975, https://doi.org/10.1016/j.foodchem.2021.129975.

[45] M. Sudhakaran, M.R. Parra, H. Stoub, K.A. Gallo, A.I. Doseff, Apigenin by targeting hnRNPA2 sensitizes triple-negative breast cancer spheroids to doxorubicin-induced apoptosis and regulates expression of ABCC4 and ABCG2 drug efflux transporters, Biochem. Pharmacol. 182 (2020) 114259, https://doi.org/10.1016/j.bcp.2020.114259.
[46] M. Ezzati, B. Yousefi, K. Velaei, A. Safa, A review on anti-cancer properties of Quercetin in breast cancer, Life Sci. 248 (2020) 117463, https://doi.org/10.1016/j.lfs.2020.117463.
[47] M. Imran, A. Rauf, T. Abu-Izneid, M. Nadeem, M.A. Shariati, I.A. Khan, A. Imran, I.E. Orhan, M. Rizwan, M. Atif, T.A. Gondal, M.S. Mubarak, Luteolin, a flavonoid, as an anticancer agent: a review, Biomed. Pharmacother. 112 (2019) 108612, https://doi.org/10.1016/j.biopha.2019.108612.
[48] Han-Tsang Wu, Joseph Lin, Yi-En Liu, Hsiao-Fan Chen, Kai-Wen Hsu, Shu-Hsuan Lin, Kai-Yen Peng, Kuo-Juei Lin, Chang-Chi Hsieh, Dar-Ren Chen, Luteolin suppresses androgen receptor-positive triple-negative breast cancer cell proliferation and metastasis by epigenetic regulation of MMP9 expression via the AKT/mTOR signaling pathway, Phytomedicine 81 (2021), https://doi.org/10.1016/j.phymed.2020.153437.
[49] X. Li, Z. Liu, J. Liao, Q. Chen, X. Lu, X. Fan, Network pharmacology approaches for research of Traditional Chinese Medicines, Chin. J. Nat. Med. 21 (5) (2023) 323–332, https://doi.org/10.1016/S1875-5364(23)60429-7.
[50] M.J. Duffy, N.C. Synnott, J. Crown, Mutant p53 in breast cancer: potential as a therapeutic target and biomarker, Breast Cancer Res. Treat. 170 (2) (2018) 213–219, https://doi.org/10.1007/s10549-018-4753-7.
[51] L. Silwal-Pandit, A. Langerod, A.L. Borresen-Dale, TP53 mutations in breast and ovarian cancer, Cold Spring Harb Perspect Med. 7 (1) (2017), https://doi.org/10.1101/cshperspect.a026252.
[52] B.D. Manning, L.C. Cantley, AKT/PKB signaling: navigating downstream, Cell 129 (7) (2007) 1261–1274, https://doi.org/10.1016/j.cell.2007.06.009.
[53] S.K. Herzog, S.A.W. Fuqua, ESR1 mutations and therapeutic resistance in metastatic breast cancer: progress and remaining challenges, Br. J. Cancer 126 (2) (2022) 174–186, https://doi.org/10.1038/s41416-021-01564-x.
[54] S. Lev, Targeted therapy and drug resistance in triple-negative breast cancer: the EGFR axis, Biochem. Soc. Trans. 48 (2) (2020) 657–665, https://doi.org/10.1042/BST20191055.
[55] J. Luo, H. Zou, Y. Guo, T. Tong, L. Ye, C. Zhu, L. Deng, B. Wang, Y. Pan, P. Li, SRC kinase-mediated signaling pathways and targeted therapies in breast cancer, Breast Cancer Res. 24 (1) (2022) 99, https://doi.org/10.1186/s13058-022-01596-y.
[56] L. Claesson-Welsh, M. Welsh, VEGFA and tumour angiogenesis, J. Intern. Med. 273 (2) (2013) 114–127, https://doi.org/10.1111/joim.12019.
[57] H. Liao, L. Zhang, S. Lu, W. Li, W. Dong, KIFC3 promotes proliferation, migration, and invasion in colorectal cancer via PI3K/AKT/mTOR signaling pathway, Front. Genet. 13 (2022) 848926, https://doi.org/10.3389/fgene.2022.848926.
[58] C. Luo, Y. Wang, C. Wei, Y. Chen, Z. Ji, The anti-migration and anti-invasion effects of Bruceine D in human triple-negative breast cancer MDA-MB-231 cells, Exp. Ther. Med. 19 (1) (2020) 273–279, https://doi.org/10.3892/etm.2019.8187.
[59] C. Wu, S. Qiu, P. Liu, Y. Ge, X. Gao, Rhizoma Amorphophalli inhibits TNBC cell proliferation, migration, invasion and metastasis through the PI3K/Akt/mTOR pathway, J. Ethnopharmacol. 211 (2018) 89–100, https://doi.org/10.1016/j.jep.2017.09.033.
[60] H. Wu, L. Chen, F. Zhu, X. Han, L. Sun, K. Chen, The cytotoxicity effect of resveratrol: cell cycle arrest and induced apoptosis of breast cancer 4T1 cells, Toxins 11 (12) (2019), https://doi.org/10.3390/toxins11120731.